COLLECTIVE EXCITATIONS AND DENSITY-WAVE INSTABILITIES IN ONE-DIMENSIONAL SOFT-CORE BOSON SYSTEMS

A THESIS SUBMITTED TO

THE GRADUATE SCHOOL OF ENGINEERING AND SCIENCE

OF BILKENT UNIVERSITY

IN PARTIAL FULFILLMENT OF THE REQUIREMENTS FOR

THE DEGREE OF

MASTER OF SCIENCE

IN

PHYSICS

By

Zohreh Mohammadi

July 2024

COLLECTIVE EXCITATIONS AND DENSITY-WAVE INSTABILITIES IN ONE-DIMENSIONAL SOFT-CORE BOSON SYSTEMS
By Zohreh Mohammadi
July 2024

We certify that we have read this thesis and that in our opinion it is fully adequate, in scope and in quality, as a thesis for the degree of Master of Science.

Bilal Tanatar (Advisor)

Hâldun Sevinçli

Engin Durgun

Approved for the Graduate School of Engineering and Science:

Orhan Arıkan
Director of the Graduate School

ABSTRACT

COLLECTIVE EXCITATIONS AND DENSITY-WAVE INSTABILITIES IN ONE-DIMENSIONAL SOFT-CORE BOSON SYSTEMS

Zohreh Mohammadi
M.S. in Physics
Advisor: Bilal Tanatar
July 2024

We investigated the dynamics of bosons interacting with Rydberg-dressed potentials in single-wire and double-wire structures. Specifically, we aimed to understand how the addition of Rydberg dressing, with its soft-core nature and van der Waals tail at long distances, influences the behavior of single-wire and double-wire systems of bosons. This investigation was conducted using the random phase approximation (RPA) and the Bogoliubov-de Gennes (BdG) mean-field approximation at zero temperature, focusing on the emergence of collective modes and density-wave instabilities.

We examined the dispersions of collective modes in single-wire and double-wire structures of bosons with Rydberg-dressed interactions. In the long-wavelength limit, symmetric and anti-symmetric modes show linear behavior in wave vectors with distinct sound velocities. A prominent maxon-roton feature appears at intermediate wave vectors, especially at large coupling constants. The influence of wire spacing on mode dispersion is significant: smaller spacings lead to the disappearance of the asymmetric mode with free-particle-like dispersion, while larger spacings result in mode degeneracy in symmetric bi-wires due to diminished inter-wire coupling. The system becomes unstable toward density-waves at strong couplings, indicated by the vanishing roton energy, affecting both symmetric and anti-symmetric branches. Additionally, density imbalances between wires shift the energy of the excitation branches and destabilize the homogeneous superfluid phase at lower coupling constants. While the roton softening observed suggests instability toward density-modulated phases, more sophisticated numerical methods are needed to characterize these phases accurately.

Keywords: Rydberg-dressed bosons, bi-wire structure, density-wave instabilities,

collective excitations.

ÖZET

BİR BOYUTLU YUMUŞAK ÇEKİRDEKLİ BOZON SİSTEMLERİNDE KOLLEKTİF UYARILAR VE YOĞUNLUK-DALGA KARARSIZLIKLARI

Zohreh Mohammadi
Fizik, Yüksek Lisans
Tez Danışmanı: Bilal Tanatar
Temmuz 2024

Rydberg giydirilmiş potansiyellerle etkileşen bozonların tek telli ve çift telli yapılardaki dinamiklerini araştırıldı. Özellikle, uzun mesafelerde yumuşak çekirdek yapısına ve van der Waals kuyruğuna sahip olan Rydberg giydirme işleminin, bozonların tek telli ve çift telli sistemlerinin davranışını nasıl etkilediğini anlamayı amaçladık. Bu araştırma, rastgele faz yaklaşımı (RPA) ve sıfır sıcaklıkta Bogoliubov-de Gennes (BdG) ortalama alan yaklaşımı kullanılarak gerçekleştirildi ve kolektif modların ortaya çıkışı ile yoğunluk dalgası kararsızlıklarına odaklandı.

Rydberg giydirilmiş etkileşimlere sahip bozonların tek telli ve çift telli yapılardaki kolektif modların dağılımlarını inceledik. Uzun dalga boyu limitinde, simetrik ve anti-simetrik modlar, farklı ses hızları ile dalga vektörlerinde doğrusal davranış sergiler. Orta dalga vektörlerinde, özellikle büyük bağlanma sabitlerinde belirgin bir maxon-roton özelliği ortaya çıkar. Tel aralığının mod dağılımı üzerindeki etkisi büyüktür: daha küçük aralıklarda, serbest parçacık benzeri dağılıma sahip asimetrik mod kaybolurken, daha büyük aralıklarda, teller arası bağlanmanın azalması nedeniyle simetrik çift telli sistemlerde mod dejenerasyonu meydana gelir. Sistem, güçlü bağlanmalarda yoğunluk dalgalarına doğru kararsız hale gelir ve bu, hem simetrik hem de anti-simetrik dallarda rotun enerjisinin yok olmasıyla gösterilir. Ayrıca, teller arasındaki yoğunluk dengesizlikleri, uyarım dallarının enerjisini kaydırır ve homojen süper akışkan fazı daha düşük bağlanma sabitlerinde kararsız hale getirir. Gözlemlenen roton yumuşaması, yoğunluk modüle edilmiş fazlara doğru bir kararsızlık önermesine rağmen, bu fazları doğru bir şekilde karakterize etmek için daha sofistike sayısal yöntemler gereklidir.

Anahtar sözcükler: Rydberg-dressed bozonlar, çift telli yapı, yoğunluk dalgası kararsızlıkları, kolektif uyarılar.

Acknowledgement

I immensely appreciate Prof. Bilal Tanatar for guiding my academic journey and providing consistent support and guidance throughout three years of dedicated research and exploration. This endeavor would not have been possible without his academic guideway and continuous help. His expertise, patience, and unwavering support have been invaluable throughout this research. His insightful feedback and guidance, from the inception of this thesis to its completion, have truly shaped the depth and quality of this work.

I extend my sincere gratitude to Bilkent University and the distinguished faculty members of the Physics Department, notably Prof. Ceyhun Bulutay, Prof. Cemal Yalabik, Prof. Mehmet Ozgur Oktel, and Prof. Oguz Gulseren for cultivating a conducive and exceptional learning environment for students to engage with advanced courses. Their commitment to academic excellence and dedication to fostering a fair and supportive atmosphere have greatly contributed to my educational experience. I am appreciative of the opportunities provided for intellectual growth and the rigorous academic standards upheld by the department, which have significantly shaped my academic journey.

I would like to extend my sincere thanks to my esteemed jury members, Prof. Hâldun Sevinçli and Prof. Engin Durgun, for generously offering their time and expertise in reading and reviewing my thesis. Their thoughtful insights, critical feedback, and constructive criticism have undoubtedly enhanced the rigor and scholarly contribution of this research. Their guidance has been instrumental in refining the arguments and analysis presented in this thesis.

I would also like to express my deep gratitude to Muhammad Hilal, a great fellow PhD student, for his invaluable assistance. His advice and insightful contributions have been instrumental in my work. I am deeply grateful for his willingness to help.

Additionally, I am deeply grateful to my family for their unwavering love, encouragement, and understanding throughout this academic journey. Their belief in me has been a constant source of motivation, particularly during the challenging phases of this research. Their support has been the bedrock upon which I could build this thesis.

Lastly, I acknowledge that the completion of this thesis would not have been achievable without the contributions and support of all these wonderful individuals. Each one has played a significant role in shaping and enriching this academic endeavor, and for that, I am profoundly thankful.

Contents

List of Figures

Chapter 1

Introduction

In recent years, there has been significant interest in Rydberg atoms [1, 2, 3]. The capability to manipulate Rydberg interactions in some systems offers a foundation for creating artificial many-body systems [4] and quantum simulators [5, 6]. Rydberg atoms have been utilized to explore a range of issues in quantum information [7, 8], quantum computation [9], and nonlinear quantum optics [10, 11]. Recently, there has been a demonstration of the collective encoding of information on Rydberg atoms. In this approach, the qubit is stored as a superposition of Rydberg polariton modes instead of being associated with a single atom [12].

Furthermore, the flexibility and tunability of Rydberg atom interactions have led to breakthroughs in studying quantum phase transitions and exotic states of matter. Experimental setups using Rydberg atoms have enabled the observation of phenomena such as topological order and quantum spin liquids. The ability to control interaction strengths and geometric configurations of Rydberg atoms provides a unique platform for investigating complex quantum systems and exploring new quantum phases that are otherwise challenging to realize in traditional condensed matter systems.

In addition to their applications in fundamental research, Rydberg atoms are being explored for their potential in practical technologies. For instance, Rydberg-based sensors have shown promise in enhancing the sensitivity and precision of measurements in electric and magnetic fields. Moreover, integrating Rydberg atoms with photonic and optomechanical systems opens new avenues for developing advanced quantum devices, including quantum transducers and interfaces for hybrid quantum networks. These developments underscore the versatile nature of Rydberg atoms and their growing impact across various quantum science and technology fields.

Rydberg states face challenges due to their short lifetimes, posing significant difficulties in utilizing them for experimental investigations of atomic dynamics [13, 14]. One potential solution to address this issue involves mixing the Rydberg state with the ground state [15, 16, 17], forming Rydberg-dressed atoms characterized by significantly extended lifetimes. The interaction among these Rydberg-dressed particles exhibits a soft-core nature and a van der Waals tail at long distances. Numerous intriguing phenomena, including the supersolid phase [18, 19], quantum liquid droplets [20, 21], clustering [22], Z_2 topological order [23], Fermi superfluid (SF) phases [24] and roton excitation [22, 25, 26], are explored using Rydberg-dressed atoms. It is proposed that rotating trapped Rydberg-dressed atoms could serve as an exceptional platform for observing the quantum Hall effect with neutral atomic gases [27] and vortex structures [28].

Furthermore, the ability to tune interactions in Rydberg-dressed systems has sparked interest in studying novel quantum phases and critical phenomena. For example, researchers are investigating the emergence of crystalline structures and stripe phases in two-dimensional Rydberg-dressed systems. These phases are characterized by their unique spatial order and collective excitations, which are not present in conventional atomic or condensed matter systems. The precise control over interaction parameters in Rydberg-dressed setups enables the exploration of phase transitions and the critical behavior associated with these exotic states.

In addition, the extended lifetimes of Rydberg-dressed atoms make them suitable candidates for implementing long-range entanglement and quantum information protocols. By leveraging these systems' tunable interactions and coherence properties, it is possible to design robust quantum gates and error-correcting codes. The versatility of Rydberg-dressed atoms also extends to simulating lattice gauge theories and exploring the dynamics of strongly correlated systems, providing insights into high-energy physics and condensed matter phenomena.

The appearance of a maxon-roton structure in the excitation spectrum is a hallmark of strongly correlated Bose liquids [15, 29, 30, 31, 32]. The theoretical prediction of a roton minimum has been made for quasi-two-dimensional dipolar Bose-Einstein condensates (BECs) within the mean-field approximation [33]. This prediction has been experimentally confirmed in Bose-Einstein condensates of highly magnetic erbium atoms [30].

The maxon-roton spectrum, characterized by a local maximum (maxon) followed by a local minimum (roton) in the excitation energy, indicates the presence of strong correlations and interactions in the system. This phenomenon has significant implications for understanding quantum fluids' collective behavior and stability. In particular, the roton minimum is associated with the tendency of the system to form density-waves or other ordered phases, which can lead to the emergence of exotic quantum states such as supersolids.

Further studies have extended the concept of roton excitations to other systems with long-range interactions, such as Rydberg-dressed atoms and dipolar gases. These investigations reveal that the interplay between interaction strength, dimensionality, and quantum fluctuations can lead to a rich variety of rotonic phenomena. For instance, tuning the interaction parameters makes it possible to transition from a stable superfluid phase to a state with periodic density modulations, highlighting the versatility of these systems in exploring new quantum phases.

The phase diagram of two-dimensional (2D) ultra-cold Rydberg-dressed bosons has been mapped out using path integral Monte Carlo simulation. This method has demonstrated that changes in density and coupling strength lead to the emergence of different phases, including superfluid and supersolid phases [18].

Path integral Monte Carlo simulations provide a powerful tool for exploring the phase behavior of complex quantum systems. By accurately accounting for quantum fluctuations and correlations, these simulations offer detailed insights into the conditions under which various quantum phases arise. The results for Rydberg-dressed bosons reveal that the interplay between particle density and interaction strength can stabilize exotic phases, which are not typically accessible in conventional condensed matter systems.

Specifically, tuning the Rydberg dressing parameters allows for precise control of the interaction potential, stabilizing supersolid phases. These phases exhibit both crystalline order and superfluidity, showcasing the unique properties of Rydberg-dressed systems. The mapping of the phase diagram further identifies critical points and phase boundaries, which are essential for understanding the transitions between different quantum states.

Moreover, the insights gained from these simulations have significant implications for experimental realizations. They guide the design of experiments to observe these novel phases, providing benchmarks and expectations for measurable quantities such as density distributions, excitation spectra, and coherence properties. The combination of theoretical predictions and experimental verifications advances our knowledge of quantum phase transitions and the role of long-range interactions in shaping the properties of quantum matter.

The dispersion of Rydberg-dressed BEC with spin-orbit coupling reveals the presence of two distinct minima corresponding to rotons. Additionally, it has been observed that the roton instability becomes more readily attainable under these conditions [34]. The excitation spectrum of Rydberg-dressed bosons has been analyzed using the hypernetted-chain Euler-Lagrange approximation. This method predicts density-wave instability within certain parameter ranges, observed in three and two dimensions [25]. Researchers have also explored the phase diagram of a two-dimensional binary Rydberg-dressed Bose-Einstein condensate within the super-solid regime [35].

We investigate the dynamics of bosons interacting with Rydberg-dressed potentials in single-wire and double-wire structures, employing the random phase approximation and the Bogoliubov-de Gennes (BdG) mean-field approximation at zero temperature. The analysis reveals a maxon-roton behavior exhibited by two collective modes corresponding to the symmetric and anti-symmetric modes of the bosonic bi-wire. When the two wires are isolated, these modes degenerate, but this degeneracy is broken by finite counterflow or density imbalance between the wires. Additionally, the study identifies the possibility of density-wave instability occurring in either or both the symmetric and anti-symmetric channels under certain values of the coupling constant and wire spacing.

We compute the collective modes of single-wire and bi-wire systems and analyze the density-wave instability for both symmetric (each wire has the same density) and density-imbalanced bi-wires (each wire has a different density).

In summary, we examine the behavior of single-wire and bi-wire systems of bosons featuring repulsive interactions influenced by soft-core Rydberg dressing. Roton minima are observed in the bi-wire's symmetric and asymmetric collective density modes. The presence of these minima depends on the boson density within each wire and the separation between the two wires.

It's important to acknowledge the extensive research on ultra-cold gases of dipolar bosons, which exhibit long-range interactions, particularly in the bi-layer setup [36, 37, 38, 39]. Predictions have been made regarding the emergence of the maxon-roton structure and density-wave instability within this system [36]. Nevertheless, nuanced discrepancies exist between dipolar and Rydberg-dressed systems. The dipole-dipole interaction is both anisotropic and long-range. The in-plane interaction becomes isotropic in a simplified scenario of perpendicularly aligned dipoles. The interaction between layers depends on the in-plane distance of dipoles and their orientation relative to the other layers. When dipole moments in two layers are parallel, the inter-layer interaction at close distances is attractive, resulting in the pairing of dipoles from different layers. This creates a compelling interplay between dipole and dimer condensations [37]. In this scenario, we expect the density-wave (DW) instability of either dipoles or dimers at extremely high densities. Another intriguing setup is a bi-layer of antiparallel dipoles, where the primary inter-layer interaction is repulsive, discouraging dimer formation. Here, a self-bound liquid formation is predicted due to the weak inter-layer attraction [39].

To observe the maxon-roton structure and roton instability in dipolar bi-layer, it is necessary to move beyond the simple BdG mean-field approximation. Even then, only the total-density mode becomes soft under strong interactions [36]. The stripe phase is favored in wire structures of tilted dipoles due to the anisotropic dipole-dipole interaction [40].

What we see in the Rydberg-dressed bi-wire highlights the importance of the interaction's soft-core and long-range characteristics. These aspects make Rydberg-dressed bi-wire distinct from dipolar bi-layer [41].

Chapter 2

Single-wire system

When examining bosons featuring repulsive soft-core Rydberg-dressed interactions confined in single-wire, the intra-wire interaction in real space is described[42].

This system is characterized by the following first-quantized Hamiltonian:

$$H = -\frac{\hbar^2}{2m} \sum_{l,i} \nabla^2_{r_i^l} + \sum_{l} \sum_{i<j} V_s \left| r_i^l - r_j^l \right| \tag{2.1}$$

In this context, m represents the mass of the particle, $l = 1$ denotes the index for the wire, r_i^l signifies the position of the ith particle in wire l, and $V_s(r)$ the intra-wire interaction in real space which will be discussed in the following[24].

2.1 Soft-core bosons in single-wire

To investigate the properties of the single-wire Rydberg-dressed system of bosons, we first consider a one-dimensional configuration, often referred to as a wire, with a specific interaction potential. The potential, denoted as $V_s(r)$, is characterized by its soft-core nature, as described by:

$$V_s(r) = \frac{U}{1 + \left(\frac{r}{R_c}\right)^6} \tag{2.2}$$

Here, r represents the distance between atoms, while U and R_c denote the interaction strength and the soft-core radius, respectively.

The parameters U and R_c are influenced by various experimental factors, including Raman coupling, red detuning, and van der Waals coefficients [13, 15, 43]. Understanding the dependence of these parameters on the interaction potential is crucial for predicting and interpreting the behavior of bosonic systems in single-wire Rydberg-dressed configurations.

The soft-core radius of interaction is $R_c = \left(\frac{C_6}{2\hbar\Delta}\right)^{1/6}$ and the interaction strength is $U = \left(\frac{\Omega}{2\Delta}\right)^4 \left|\frac{C_6}{R_c^6}\right|$.

Here Ω, $\Delta < 0$, and $C_6 < 0$ are the effective Raman coupling, red detuning, and averaged van der Waals coefficient, respectively[21].

These equations establish the essential relationships between the parameters governing the interaction potential in the single-wire Rydberg-dressed system of bosons. The soft-core radius of interaction, denoted as R_c, is determined by the averaged van der Waals coefficient C_6 and the red detuning Δ. Additionally, the interaction strength U depends on the same parameters along with the effective Raman coupling Ω.

Understanding the interplay between these parameters is crucial for characterizing the behavior of bosonic systems in single-wire Rydberg-dressed configurations. In particular, the soft-core radius R_c delineates the range over which the interaction potential exhibits significant effects, while the interaction strength U quantifies the overall strength of inter-particle interactions within the system.

In Figure 2.1, we show $V_s(r)$ versus $\frac{r}{R_c}$. It provides a visual representation of

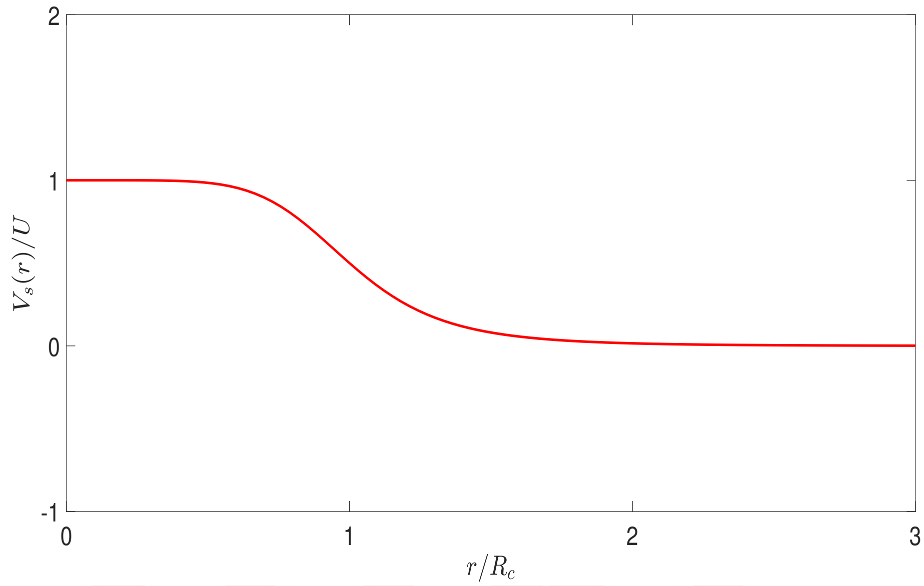

Figure 2.1: The intra-wire Rydberg-dressed interaction $V_s(r)$. Plot of $V_s(r)$ versus $\frac{r}{R_c}$, where $V_s(r)$ is scaled by U

the interaction potential $V_s(r)$ as a function of $\frac{r}{R_c}$, where r denotes the distance between particles and R_c represents the soft-core radius of interaction. This dimensionless representation allows for a clear illustration of the behavior of the potential over a range of distances scaled by the characteristic length R_c.

Furthermore, to gain insight into the reciprocal space representation of the interaction potential, we computed the Fourier transform of $V_s(r)$, considering momentum transfer q scaled by R_c ($qR_c = \tilde{q}$). This analysis provides valuable information about the spatial periodicity and momentum distribution of the interaction potential, shedding light on the characteristic momentum scales associated with the system.

By examining both the real-space and reciprocal-space representations of $V_s(r)$, we gain a comprehensive understanding of the spatial and momentum characteristics of the interaction potential, which are essential for elucidating the energy and momentum transfer dynamics within the single-wire Rydberg-dressed system of bosons.

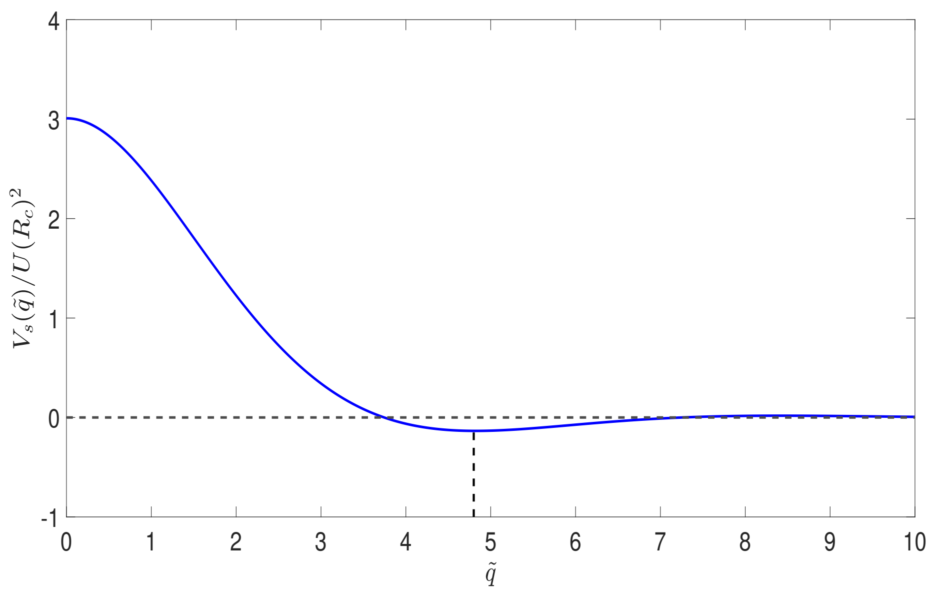

Figure 2.2: The Fourier transforms of the intra-wire Rydberg-dressed interaction $V_s(\tilde{q})$. Plot of $V_s(\tilde{q})$ versus $\tilde{q} = qR_c$, where $V_s(\tilde{q})$ is scaled by $U(R_c)^2$.

To further analyze the characteristics of the interaction potential in reciprocal space, we computed the Fourier transform of $V_s(r)$, with momentum transfer q scaled by R_c ($qR_c = \tilde{q}$). This transformation allows us to examine the wavevector dependence of the potential, providing insights into its behavior at different momentum scales.

$$V_s(\tilde{q}) = \frac{UR_c\pi}{3}\left(\cos\left(\frac{\sqrt{3}}{2}\tilde{q}\right) + \exp\left(-\frac{\tilde{q}}{2}\right) + \sqrt{3}\sin\left(\frac{\sqrt{3}}{2}\tilde{q}\right)\right)\exp\left(-\frac{\tilde{q}}{2}\right) \quad (2.3)$$

Figure 2.2 presents $V_s(\tilde{q})$ as a function of $\tilde{q}$, with $V_s(\tilde{q})$ scaled by $U(R_c)^2$. This scaling facilitates a clear visualization of the wavevector dependence of the interaction potential, highlighting the relative strength of interactions at different momentum transfers.

The analysis of $V_s(\tilde{q})$ in reciprocal space complements our understanding of the real-space interaction potential, offering valuable information about the spatial periodicity and momentum distribution of the interactions within the single-wire

Rydberg-dressed system of bosons.

The behavior depicted in Figures 2.1 and 2.2 offers a comprehensive view of the effective Rydberg-dressed potential, elucidating its characteristics in both position and momentum spaces. These visual representations provide valuable insights into the spatial periodicity and momentum distribution of the interparticle interaction within the single-wire Rydberg-dressed system of bosons.

The Fourier transform of the intra-wire interaction reveals intriguing features, notably the presence of negative minima at finite wavevectors. Specifically, the minimum for $V_s(\tilde{q})$ occurs at $\tilde{q}_{min} \approx 4.8$. This observation holds significant implications for the system's behavior [33]. The existence of these negative minima in the interaction potential is pivotal for the emergence of minima in the roton spectrum and the onset of instability in the homogeneous phase of the system.

It's important to note that our analysis considers an idealized scenario where the finite width of the wire is not taken into account. This simplification is justified when the width of the wire is significantly smaller than the soft-core radius R_c, ensuring that the effects of wire confinement on the interaction potential are negligible. This approximation allows us to focus on the intrinsic characteristics of the interparticle interaction, facilitating a clearer understanding of its role in shaping the collective behavior of bosons within the system.

2.1.1 Analysis of the interaction potential in both position and momentum space

We delve into a comprehensive analysis of the behavior of the interaction potential within the single-wire Rydberg-dressed system of bosons, focusing on both position and momentum space representations. Our investigation reveals intriguing insights into the interplay between short-range repulsion and long-range attraction, shedding light on the underlying mechanisms governing the collective behavior of bosons in this system.

We begin by examining the distinct characteristics of the interaction potential in position space, highlighting its behavior at different length scales and elucidating its purely repulsive nature within the characteristic range. Subsequently, we turn our attention to the Fourier transform of the interaction potential, unveiling unexpected features such as negative minima, which deviate from the typical behavior observed in long-range interactions.

Through a detailed interpretation of these observations, we uncover the role of the dipole-blockade effect in driving the emergence of attractive contributions in momentum space, despite the repulsive nature of the interaction in position space. This delicate balance between repulsion and attraction holds significant implications for the collective dynamics of bosons in the system, offering new avenues for exploration and understanding.

In the following, we systematically analyze the position and momentum space behaviors of the interaction potential, discuss their physical implications, highlight their significance in the broader context of quantum systems, and explore potential applications in experimental settings.

1. **Position Space Behavior**

   The interaction potential in position space exhibits distinct characteristics:

   - For $r < R_c$, the interaction potential is nearly flat, indicating a short-range repulsive interaction.
   - Beyond $r > R_c$, a van der Waals tail emerges, signifying a long-range interaction decaying as $1/r^6$.
   - Importantly, within the characteristic range $r < R_c$, the interaction is purely repulsive.

2. **Momentum Space (Fourier Transform) Behavior**

   The Fourier transform of the interaction potential, denoted as $V_s(\tilde{q})$, reveals intriguing behavior:

   - It exhibits a negative minimum at $\tilde{q} \approx 4.8$.

- This peculiar behavior is not commonly observed in other types of long-range interactions.

3. **Interpretation of Physical Implications**

   The dipole-blockade effect is a phenomenon where the presence of one dipole in a system inhibits the excitation of neighboring dipoles. It underlies the observed behavior:

   - Observing the negative minimum in $V_s(\tilde{q})$ at $\tilde{q} \approx 4.8$.
   - The negative minimum indicates a region in momentum space where the interaction becomes more attractive.
   - This attraction at $\tilde{q} \approx 4.8$ is a consequence of the dipole-blockade effect overcoming the purely repulsive nature of the interaction in position space.
   - It suggests a delicate balance between the repulsive forces dominating at short distances in position space and an attractive contribution emerging at specific momentum values.

4. **Significance**

   - Unusual Nature: This behavior is unique, with a repulsive position space potential and an attractive momentum space Fourier transform.
   - Importance of Fourier Transform: The Fourier transform provides a valuable perspective, revealing hidden features and transitions between repulsion and attraction.
   - Distinct from Typical Long-Range Interactions: Unlike typical long-range interactions, which often exhibit monotonic decay or oscillations, this system's interaction shows a negative minimum due to the dipole-blockade effect.

5. **Applications**

   - Quantum Systems: Understanding such behavior is crucial in quantum systems, where long-range interactions play a significant role.

- Cold Atom Systems: Dipole-blockade effects are particularly relevant in cold atom systems, where atoms are in highly excited states.
- Experimental Verification: The observed behavior in $V_s(\vec{q})$ can be experimentally verified through scattering experiments, providing validation for theoretical models.

In summary, the negative minimum in the Fourier transform of the interaction potential, arising from the dipole-blockade effect, signifies a transition from repulsive to attractive behavior in momentum space. This behavior, unique to the system under study, highlights the intricate interplay between short-range repulsion and long-range attraction, with implications for various quantum and cold atom systems. It underscores the importance of considering both position and momentum space representations to comprehend the complex nature of interparticle interactions fully.[20, 42]

2.2 Bogoliubov-de Gennes (BdG) equations

Adding the BdG equations and discussing them in the context of our text can provide further depth to our analysis. Here's how we can integrate them:

The BdG equations, widely employed in the study of superfluids and superconductors, offer a powerful framework for understanding the behavior of quasiparticles in the presence of interactions. In our investigation of Rydberg-dressed bosons confined in single-wire, integrating the BdG equations provides a deeper insight into the collective excitations of the system and its stability properties.

By solving the BdG equations, we gain the ability to explore the collective excitations of the single-wire system, taking into account the intricate interplay between kinetic energy, interaction effects, and external potentials. This enables us to assess the system's response to perturbations and predict its dynamic behavior under various conditions.

Of particular interest is the application of the BdG equations across different regimes of the Bose gas. In regimes where interactions are negligible, such as the harmonic oscillator regime, the behavior of the system is dominated by kinetic energy. However, our focus lies on the Thomas-Fermi regime, characterized by a large number of particles with strong interactions.

In this regime, the BdG equations provide invaluable insights, as they allow us to disregard the condensate's kinetic energy relative to the interaction and trapping energies. This simplification facilitates the analysis of the system's behavior under the influence of strong interactions, offering a deeper understanding of its collective dynamics.

This approach follows de Gennes [44], which involves expanding the field operator $\hat{\Psi}(x)$ in terms of Bogoliubov modes. This expansion, as given by Equation (2.4), represents a canonical transformation, provided that the Bogoliubov amplitudes $U_\nu(x)$ and $V_\nu(x)$ satisfy a crucial orthogonality condition, as specified by Equation (2.5).

$$\delta\hat{\Psi}(x) = \sum\nolimits_{\nu}' (U_\nu(x)\hat{\alpha}_\nu + V_\nu^*(x)\hat{\alpha}_\nu^\dagger) \tag{2.4}$$

The operators $\hat{\alpha}_\nu^\dagger$ and $\hat{\alpha}_\nu$ correspond to creation and annihilation operators, respectively, obeying bosonic commutation relations. Here, the Bogoliubov modes indexed by ν represent collective excitations of the system, with the exclusion of the ground state $|0\rangle$, indicated by the prime notation in the summation.

The orthogonality condition ensures that the resulting Hamiltonian, derived from the expansion in Equation (2.4), becomes diagonal. This diagonalization is achieved by satisfying the BdG equations, which relate the Bogoliubov amplitudes $U_\nu(x)$ and $V_\nu(x)$ to the energy spectrum of the system.

$$\int d^3x\, (U_\nu^*(x)U_{\nu'}'(x) - V_\nu^*(x)V_{\nu'}'(x)) = \delta_{\nu\nu'} \tag{2.5}$$

We will impose this condition accordingly. Subsequently, the resulting Hamiltonian will be diagonal if the functions satisfy the BdG equations:

$$
\begin{aligned}
\left(\epsilon_\nu - H_{\mathrm{Fl}}(x)\right) U_\nu(x) &= \int d^3y\, V_{\mathrm{int}}\,(x-y)\left(\Psi(y)\Psi(x)V_\nu(y) + \Psi^*(y)\Psi(x)U_\nu(y)\right) \\
-\left(\epsilon_\nu + H_{\mathrm{Fl}}(x)\right) V_\nu(x) &= \int d^3y\, V_{\mathrm{int}}\,(x-y)\left(\Psi(y)^*\Psi(x)^*U_\nu(y) + \Psi(y)\Psi^*(x)V_\nu(y)\right)
\end{aligned}
\tag{2.6}
$$

where ϵ_ν represents the excitation energy of mode ν. In the equations provided, we have introduced the definition of the fluctuation Hamiltonian density as follows:

$$
H_{\mathrm{Fl}}(x) = h_0(x) - \mu + \int d^3y \Psi^*(y) V_{\mathrm{int}}\,(x-y)\,\Psi(y) \tag{2.7}
$$

Certainly, it's necessary to treat the BdG equations (2.6) separately within and outside the condensate. Within the condensate, the solution for the external region implies $V_\nu(x) = 0$. Consequently, both the depletion and the correction to the ground-state energy vanish entirely in this region. Therefore, we confine our analysis to the condensate region. Under these conditions, the BdG equations are simplified to:

$$
\begin{aligned}
\left(\epsilon_\nu + \frac{\hbar^2\Delta^2}{2M}\right) U_\nu(x) &= \int d^3y\, V_{\mathrm{int}}(x-y)\left(\Psi(y)\Psi(x)V_\nu(y) + \Psi^*(y)\Psi(x)U_\nu(y)\right) \\
-\left(\epsilon_\nu + \frac{\hbar^2\Delta^2}{2M}\right) V_\nu(x) &= \int d^3y\, V_{\mathrm{int}}(x-y)\left(\Psi(y)^*\Psi(x)^*U_\nu(y) + \Psi(y)\Psi^*(x)V_\nu(y)\right)
\end{aligned}
\tag{2.8}
$$

We will analytically solve this set of coupled equations for two cases: a homogeneous dipolar Bose gas and a harmonically trapped gas, both within the semiclassical approximation.

Because of translation invariance, momentum becomes a conserved quantum number, allowing us to label excitations with the wave vector k. In this scenario, the Bogoliubov equations (2.8) simplify to algebraic equations in Fourier space, expressed as:

$$\epsilon_K U_K = \epsilon_{0K} U_K + nV_{\text{int}}(K)(U_K + V_K) \tag{2.9}$$

$$-\epsilon_K V_K = \epsilon_{0K} V_K + nV_{\text{int}}(K)(U_K + V_K) \tag{2.10}$$

where $\epsilon_{0K} = \frac{\hbar^2 K^2}{2M}$ and appropriate algebraic manipulations enable the solution for both the Bogoliubov amplitudes:

$$V_K^2 = \frac{1}{2\epsilon_K}(\epsilon_{0K} + nV_{\text{int}}(K) - \epsilon_K) \tag{2.11}$$

And the Bogoliubov spectrum:

$$\epsilon_K = \sqrt{\epsilon_{0K}^2 + 2n\epsilon_{0K} V_{\text{int}}} \tag{2.12}$$

We delve deeper into how solving the BdG equations and applying them can provide insight into the behavior of our system of soft-core Rydberg-dressed bosons in single-wire.

In our system, the BdG equations capture the collective excitations arising from the interactions between Rydberg-dressed bosons. These equations are derived from the mean-field approximation and provide a way to study the emergence of quasiparticle excitations, which are a hallmark of many-body systems.

1. **Collective modes:** Collective modes can reveal important information about the dynamics of our system, such as the presence of roton minima and density-wave instabilities. For instance, in the context of our research, the BdG equations can elucidate how the soft-core Rydberg-dressed interactions influence the dispersion relation of these collective modes.

2. **Effects of Rydberg dressing:** By incorporating the Rydberg-dressed interactions into the BdG equations, we can analyze how these interactions modify the behavior of the collective modes compared to systems without Rydberg dressing. This could include investigating how the soft-core nature of the interactions affects the stability of the system and the emergence of novel phenomena such as supersolid phases or roton instabilities.

3. **Wire structure:** Since our system also involves a double-wire structure in the following chapter, the BdG equations allow us to study the interplay between intra-wire and inter-wire interactions, providing insights into the coupling between the two wires and the resulting collective excitations.

2.3 Random phase approximation (RPA)

The random phase approximation is a valuable method for studying the collective excitations of many-body systems. In our context, we can apply RPA to investigate the system's dynamic structure factor and susceptibility. By treating fluctuations around the mean field, RPA allows us to explore the stability and response of the system to perturbations.

Incorporate the RPA framework into our discussion by mentioning how it can be utilized to analyze the density-wave instability and other collective phenomena observed in our Rydberg-dressed boson system. We can highlight how RPA provides a theoretical framework for understanding experimental observations and predicting novel phenomena in our system.

By integrating the BdG equations and discussing the RPA, we can enhance the theoretical framework of our research and provide a comprehensive analysis of the collective behavior of soft-core Rydberg-dressed bosons in our single-wire system.

We delve deeper into how applying the RPA can provide insight into the behavior of our system of soft-core Rydberg-dressed bosons in single-wire.

The RPA is a powerful method for probing the dynamic response of many-body systems to external perturbations. In our study of soft-core Rydberg-dressed bosons, RPA can be applied to analyze the system's susceptibility and dynamic structure factor.

1. **Susceptibility:** RPA allows us to calculate our system's susceptibility, which quantifies its response to external fields or fluctuations. By examining how the susceptibility changes with parameters such as boson density and interaction strength, we can predict the occurrence of phase transitions or instability phenomena, such as density-wave instabilities.

2. **Dynamic structure factor:** By applying RPA to the dynamic structure factor, we can investigate the collective excitations and spectral properties of our system. This analysis provides valuable information about the dispersion relation of collective modes and can help identify characteristic features such as roton minima or soft modes associated with density-wave instabilities.

3. **Comparison with experiments:** RPA predictions can be compared with experimental measurements, validating theoretical models and offering insights into the underlying physics of Rydberg-dressed boson systems. Discrepancies between theory and experiment can highlight areas where further theoretical development or experimental investigation is needed.

In summary, by incorporating the BdG equations and RPA into our analysis, we can gain a deeper understanding of the collective behavior of soft-core Rydberg-dressed bosons in our single-wire system. These theoretical frameworks allow us to explore the influence of Rydberg dressing on collective excitations, predict novel phenomena, and provide valuable guidance for experimental studies[45, 46, 47].

2.3.1 RPA formalism for double-wire systems

The RPA is a powerful and widely used method in many-body physics for analyzing collective excitations and response functions in interacting systems. When applied to double-wire systems, RPA provides a framework to study the complex interplay between the wires' density fluctuations and the resultant instabilities.

Double-wire systems consist of two parallel wires. These systems are of great interest due to the rich interplay of inter-wire and intra-wire interactions. The coupling between the wires can lead to new and intriguing phenomena, including density-wave instabilities, which are the focus of this study.

In the RPA framework, the collective excitations of the system are described by summing an infinite series of bubble diagrams. This approximation effectively accounts for the screening effects of particle-particle interactions, which are crucial for understanding the response of the system to external perturbations.

For a double-wire system, the total density response function $\chi(q,\omega)$ can be written in terms of the intra-wire V_s and inter-wire V_d and χ_0 density response functions. These functions describe the density fluctuations within and between the wires, respectively.[24, 36]

The poles of the total density response function $\chi(q,\omega)$ correspond to the collective modes of the system. These poles can indicate the presence of density-wave instabilities.

In practical applications, solving the RPA equations often requires numerical techniques due to the complexity of the interactions and the response functions. By discretizing the momentum and frequency space, one can compute the response functions and solve for the collective modes numerically. This approach allows for detailed studies of the density-wave instabilities and their dependence on various parameters such as inter-wire distance, interaction strength, and electron density.[40, 42]

The RPA formalism provides a robust framework for analyzing density-wave instabilities in double-wire systems. By considering both intra-wire and inter-wire interactions, RPA captures the essential physics governing the collective excitations in these systems. The resulting density-wave instabilities offer insights into the emergent behavior of coupled one-dimensional electron gases and highlight the intricate interplay between correlation effects and dimensionality.

2.4 Density-density response function

The study of collective density modes and the identification of signatures indicating the instability of a homogeneous system towards density-modulated phases are crucial aspects of condensed matter physics. These phenomena can be effectively characterized through the analysis of the density-density response function, which encapsulates the system's dynamic response to perturbations in density.

The density-density response function serves as a fundamental tool in theoretical investigations, providing valuable insights into the underlying interactions and collective behavior of particles in the system. Singularities in the response function reveal essential information about the emergence of collective excitations and phase transitions, shedding light on the complex interplay between various physical parameters.

In this section, we delve into the formalism governing the density-density response function, exploring its mathematical representation and the physical implications of its singularities.

The collective density modes and signatures of the instability of a homogeneous system to density-modulated phases both could be obtained from the singularities of its density density response function, respectively, in the dynamic and static regimes.

$$\chi(q,\omega) = \frac{\chi_0(q,\omega)}{1 - V_s(q)\chi_0(q,\omega)} \tag{2.13}$$

Utilizing the RPA, we undertake an investigation into the density wave instability (DWI). This analysis hinges on discerning the poles of its static density-density response function or, equivalently, identifying the zeros of its static dielectric function. Through this approach, we aim to unravel the intricate dynamics underlying the emergence and evolution of the DWI phenomenon. By scrutinizing both the static and dynamic characteristics, we seek to elucidate the underlying mechanisms governing the transition towards density-modulated phases, offering invaluable insights into the collective behavior of the system.

$$1 - V_s(q)\chi_0(q,\omega) = 0 \tag{2.14}$$

The $\chi_0(q,\omega)$ represents the zero-temperature, non-interacting density-density response function, serving as a foundational element in characterizing its collective behavior. Concurrently, $V_s(q)$ denotes the intra-wire interaction potential within the system. Through rigorous analysis of these components, we aim to delineate the intricate interplay between the non-interacting response function and the intra-wire interaction potential, elucidating their collective influence on the dynamic and thermodynamic properties of the system.

$$\chi_0(q,\omega) = \frac{2n\epsilon_q}{\hbar^2\omega^2 - \epsilon_q^2} \tag{2.15}$$

Here, ϵ_q represents the dispersion relation of free bosons, encapsulating the energy-momentum relationship within the system. Additionally, n denotes the particle density, quantifying the number of bosons per unit volume.

$$\epsilon_q = \frac{\hbar^2 q^2}{2m} \tag{2.16}$$

In order to compute the excitation spectrum, we employ the BdG approximation, a powerful framework widely utilized in the study of bosonic systems. Within this approximation, the quasiparticle excitation spectrum is rigorously formulated as [48]:

$$\hbar\omega = \hbar\omega(q) \tag{2.17}$$

$$\hbar\omega(q) = \sqrt{\epsilon_q^2 + 2n\epsilon_q V_s(q)} \tag{2.18}$$

It is worth noting that the excitation spectrum derived from the BdG approximation is equivalent to the dispersion of collective modes within the RPA framework. This equivalence underscores the robustness and versatility of both methodologies in capturing the dynamic behavior of bosonic systems [49].

Here, a more comprehensive description of our system can be attained through the introduction of a key parameter, namely the dimensionless parameter describing interaction:

$$\alpha = \frac{nmR_c^3U}{\hbar^2} \tag{2.19}$$

In Figure 2.3, we present a graphical representation illustrating the dependence of $\hbar\omega(q)$ on $\tilde{q}$ for different values of the parameter α. Here, $\hbar\omega(q)$ is appropriately scaled by the characteristic energy $E_0 = \frac{\hbar^2}{2mR_c^2}$. Notably, our analysis reveals distinct trends with increasing values of α: particularly, for stronger soft-core interactions, a notable shift of the roton mode towards the instability point is observed. This observation underscores the significant influence of interaction strength on the dynamic behavior and stability characteristics of the system. Through systematic exploration of parameter space, we aim to unravel the intricate interplay between interaction potentials and system dynamics, offering valuable insights into the emergence of collective modes and phase transitions in soft-core bosonic systems.

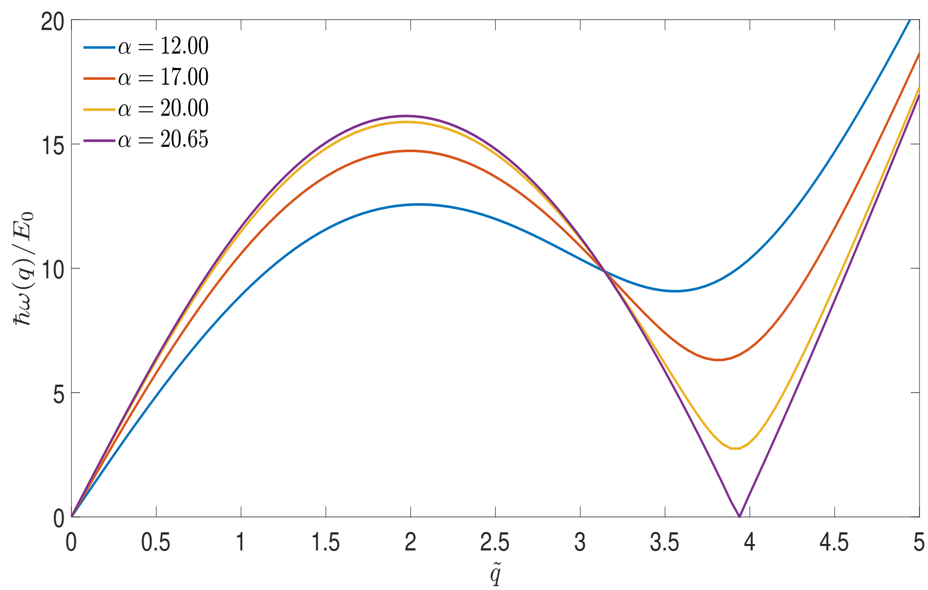

Figure 2.3: Dispersion plot of $\hbar\omega(q)$ vs. $\tilde{q}$ for various values of α, where $\hbar\omega(q)$ is scaled by $E_0 = \frac{\hbar^2}{2mR_c^2}$.

When $\hbar\omega(q) = 0$, it signifies the existence of a mode within the excitation spectrum possessing zero energy at a specific wavevector q. This occurrence denotes a critical point in the dispersion relation, where the collective excitations of the system become gapless. In the realm of condensed matter physics, such points hold significant importance as they are frequently linked with phase transitions or instabilities within the system. The emergence of a gapless mode signifies a fundamental change in the dynamic behavior of the system, often heralding the onset of novel phases or critical phenomena. By identifying and analyzing these critical points, we gain invaluable insights into the underlying mechanisms driving the collective behavior and phase transitions exhibited by condensed matter systems, thereby advancing our understanding of their rich and diverse phenomenology.

In the context of the density wave instability (DWI) being investigated here, the point where $\hbar\omega(q) = 0$ indicates the onset of an instability towards a new phase. Let's consider what happens when this condition is met:

At $\hbar\omega(q) = 0$

- Instability point: At $\hbar\omega(q) = 0$, the excitation energy for the system at wavevector q becomes zero. This implies that the system can lower energy by exciting collective modes with this wavevector.

- Critical behavior: This zero-energy mode often signifies the system's approach to a critical point, where small perturbations can lead to large-scale changes in the system's behavior, reflecting its heightened sensitivity to external influences.

Implications and phase transitions

- Phase Transition: The DWI occurs when the system becomes unstable towards the formation of a spatially modulated phase. This instability leads to the condensation of bosons at a non-zero wavevector, indicating a transition to a new phase with a broken symmetry.

- Formation of a condensate: At this critical point, bosons start to condense at a particular wavevector, indicating the formation of a periodic density modulation in the system.

- Emergence of order: The appearance of this zero-energy mode suggests that the system is favoring a certain spatial ordering, where density fluctuations at this wavevector become dominant.

Discussion of the figure

In the provided figure, $\hbar\omega(q)$ is scaled by $E_0 = \frac{\hbar^2}{2mR_c^2}$, and it's plotted against $\tilde{q}$ for various values of α. When $\hbar\omega(q) = 0$, the scaled excitation energy is zero.

- At $\hbar\omega(q) = 0$: If we observe points on the plot where $\hbar\omega(q) = 0$, these correspond to the points where the excitation energy is zero, indicating the onset of the DWI.

- Critical α: For each curve corresponding to a specific α, the point where $\hbar\omega(q) = 0$ marks the critical $\tilde{q}$ at which the system becomes dynamically unstable. This is often the point where the phase transition occurs.

- Behavior with α: As α increases, the critical $\tilde{q}$ for the instability may shift. Higher values of α correspond to stronger interactions, which can stabilize or destabilize different phases.

  In summary, when $\hbar\omega(q) = 0$ in the context of the DWI, it indicates the system's transition to a new phase characterized by the condensation of bosons at a specific wavevector. This zero-energy mode signals the onset of instability and marks a critical point where the system undergoes a phase transition, often associated with the emergence of spatial ordering and broken symmetry. The provided plot helps visualize how this behavior changes with varying dimensionless interaction parameter α values.

2.5 Density-wave instability

When investigating the density-wave instability, a crucial component is the density-density response function, denoted as:

$$\chi(q) = \frac{\chi_0(q)}{1 - V_s(q)\chi_0(q)} \tag{2.20}$$

where $\chi_0(q, \omega = 0) = \chi_0(q)$ is the static limit of the non-interacting density-density response function.

$$\chi_0(q) = -\frac{2n}{\epsilon_q} \tag{2.21}$$

where ϵ_q is the dispersion of free bosons, and n is the particle density in each wire (assumed to be the same for both wires).

The dispersion relation for free bosons is given by:

$$\epsilon_q = \frac{\hbar^2 q^2}{2m} \tag{2.22}$$

In Figure 2.4, we present a plot of $-\chi(q)UR_c$ versus $\tilde{q} = qR_c$ for different values of α. This graphical representation offers crucial insights into the behavior of the system, with particular emphasis on the divergence observed at a specific value of $\alpha = \alpha_c$.

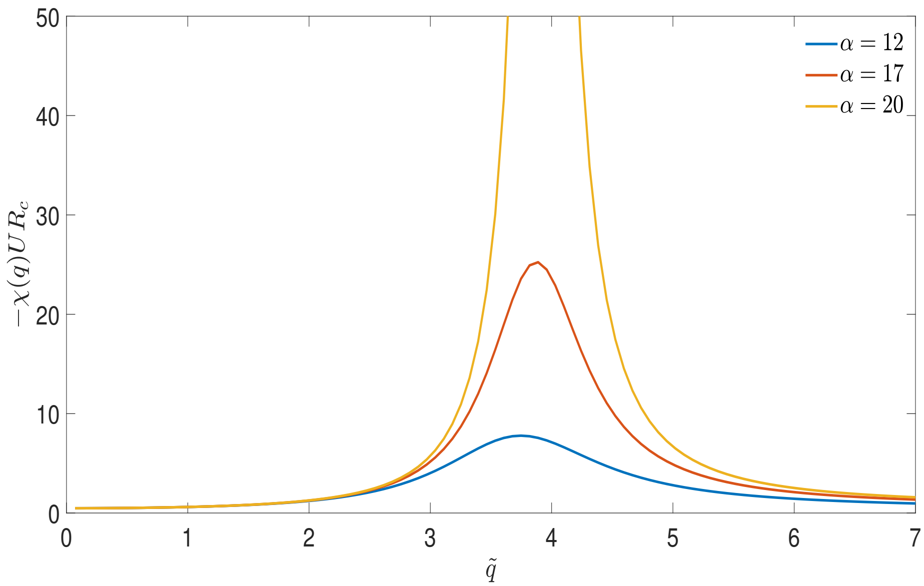

Figure 2.4: The density-density response function [in the units of $1/UR_c$] within the random phase approximation. Plot of $-\chi(q)UR_c$ Versus $(\tilde{q}) = qR_c$ for various values of α.

Figure 2.4 reveals important information about the system's behavior, particularly the divergence behavior at a specific value of $\alpha = \alpha_c$. Here, we discuss what this divergence signifies:

- The plot indicates that as α approaches a critical value α_c, the quantity $-\chi(q)UR_c$ diverges. It is the point that roton is vanishing.
- The divergence of $-\chi(q)UR_c$ at $\alpha = \alpha_c$ suggests the presence of a critical point in the system.
- This critical point is often associated with a phase transition, where the system undergoes a qualitative change in behavior.
- This divergence indicates the onset of instability in the system.

- The system becomes increasingly unstable towards a phase transition as α approaches α_c.
- The divergence signifies the emergence of strong collective effects in the system.
- These collective effects are a result of the interplay between the density-density response and the interaction strength.
- The divergence at α_c often signals the breakdown of any mean-field approximation that might have been used.
- As α crosses α_c, the system transitions from a regime where mean-field theories are valid to a regime where strong fluctuations and collective effects dominate.
- This divergence indicates that the system is undergoing a phase transition, potentially towards a state with broken symmetry or new collective behavior.

In summary, the divergence of $-\chi(q)UR_c$ in Figure 2.4 as α approaches a critical value α_c signifies the onset of a phase transition. This behavior indicates the breakdown of mean-field theories, the emergence of strong collective effects, and the system's transition to a new state with possibly broken symmetry. The plot helps visualize how the behavior of the system changes as the interaction strength parameter α is varied, highlighting the critical point where the system undergoes a qualitative change.

2.5.1 Density-wave instabilities in various systems

Density-wave instabilities are a fascinating phenomenon observed in a wide range of physical systems beyond the one-dimensional soft-core boson systems that are the focus of this study. These instabilities represent a fundamental aspect of many-body physics, where the collective behavior of particles leads to spontaneous symmetry breaking and the formation of periodic structures in the density profile.

Charge density-waves in solids

One of the most well-known examples of density-wave instabilities is the formation of charge density-waves (CDWs) in low-dimensional solids, particularly in quasi-one-dimensional materials. In these systems, electron-phonon interactions can lead to a periodic modulation of the electron density, accompanied by a distortion of the underlying lattice. The competition between electron-electron interactions and the kinetic energy of the electrons drives the system into a state where the density-wave is energetically favorable.

Spin density-waves in magnetic systems

In magnetic systems, spin density-waves (SDWs) can occur, which are analogous to CDWs but involve periodic modulations of the spin density instead of the charge density. These instabilities are often found in antiferromagnetic materials, where the exchange interactions between localized magnetic moments lead to a spatially varying spin structure.[50, 51, 52]

Density-waves in cold atomic gases

In recent years, cold atomic gases have emerged as an excellent platform for studying density-wave instabilities under highly controlled conditions. Bose-Einstein condensates (BECs) and degenerate Fermi gases confined in optical lattices can exhibit various types of density-wave phases depending on the interatomic interactions and the dimensionality of the system. For instance, in one-dimensional optical lattices, bosonic atoms with soft-core interactions can form density-wave patterns due to the interplay between kinetic energy, interaction energy, and external confinement. These systems provide a versatile testbed for exploring the fundamental principles of density-wave formation and the associated quantum phase transitions.

Electron hole bi-layers

In semiconductor systems, electron-hole bi-layers can exhibit density-wave instabilities known as excitonic density-waves. These occur when electron and hole gases, confined in adjacent layers, form bound states (excitons) due to Coulomb attraction. Under appropriate conditions, these excitons can condense into a state that exhibits a periodic modulation in the density of excitons.[53, 54, 55, 56]

Density-waves in quantum hall systems

Quantum Hall systems offer another intriguing context for density-wave instabilities. In the fractional quantum Hall regime, the competition between Coulomb interactions and the kinetic energy of electrons in high magnetic fields can lead to the formation of charge density-wave states. These states exhibit periodic electron density modulations and are a hallmark of strong correlations in two-dimensional electron systems.

Density-waves in high-energy Physics

Density-wave instabilities are not limited to condensed matter systems; they also appear in the context of high-energy physics. In the quark-gluon plasma, which is believed to have existed shortly after the Big Bang, density-waves can manifest as oscillations in the quark density. These waves are linked to the non-trivial vacuum structure of quantum chromodynamics (QCD) and play a crucial role in understanding the dynamics of the early universe and the behavior of strongly interacting matter at extreme conditions.

In conclusion, the occurrence of density-wave instabilities across such diverse systems highlights their fundamental nature in many-body physics. Whether in low-dimensional solids, magnetic materials, cold atomic gases, quantum Hall systems, or high-energy physics, the underlying mechanisms leading to the formation of density-waves share common principles. These instabilities are a testament to the rich and complex behavior that emerges from the collective interactions of particles, providing deep insights into the organization and dynamics of matter.[57, 58, 59, 60]

By recognizing and studying these universal aspects of density-wave instabilities, we can gain a more comprehensive understanding of the various physical systems in which they arise. This broader perspective enriches our knowledge of phase transitions, symmetry breaking, and the emergent phenomena that characterize complex many-body systems.

2.6 Long wavelength excitations and sound velocity

It follows from Eq. (2.18) that in the long wavelength limit, the dispersion is linear when q approaches zero.

$$\omega(q \to 0) \approx \nu_s q \tag{2.23}$$

where ν_s is the sound velocity, and using the exact expression for the Fourier transform of the Rydberg-dressed potential,$V_s(q)$ Eq. (2.3), we obtain $V_s(q \to 0)$ and therefore:

$$\nu_s = \sqrt{\frac{nV_s(q \to 0)}{m}} \tag{2.24}$$

$$\nu_s = \left(\sqrt{\frac{2}{3}\pi\alpha}\right)\nu_c \tag{2.25}$$

where ν_c is the characteristic velocity:

$$\nu_c = \frac{\hbar}{mR_c} \tag{2.26}$$

Utilizing the RPA, we delve into the investigation of the DWI. Our analysis focuses on discerning the poles of its static density-density response function or, equivalently, identifying the zeros of its static dielectric function, denoted as $F(q)$:

$$F(q) = 1 - V_s(q)\chi_0(q) \tag{2.27}$$

By employing the RPA framework, we aim to elucidate the intricate dynamics underlying the emergence and evolution of the DWI phenomenon. The static dielectric function $F(q)$ serves as a pivotal indicator, providing insights into the system's susceptibility to density fluctuations and the onset of instability towards density-modulated phases. Through systematic exploration of the poles and zeros of $F(q)$, we seek to unravel the underlying mechanisms governing the DWI and the transition towards spatially modulated phases. This approach enables us to gain a comprehensive understanding of the collective behavior, shedding light on its rich phenomenology and potential applications in diverse physical contexts.

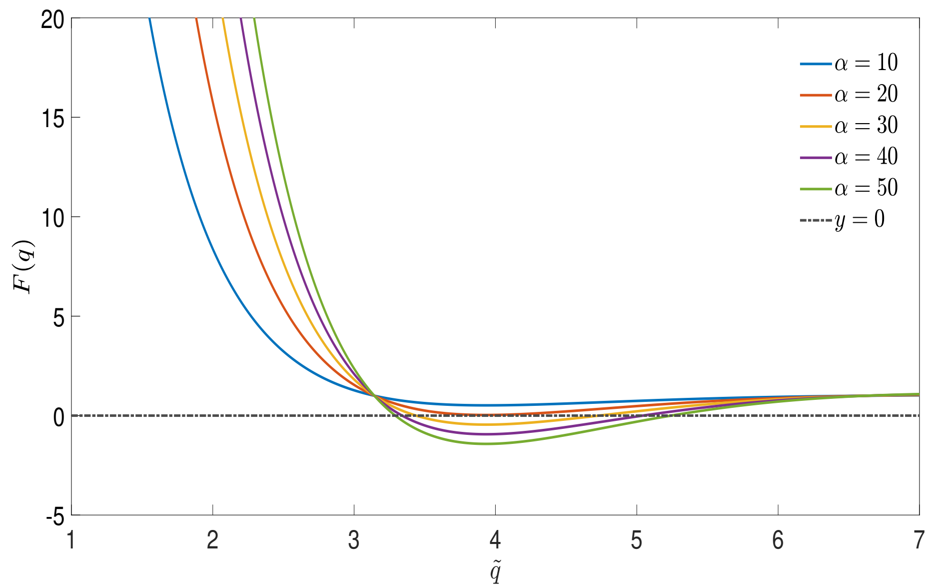

Figure 2.5: Plot of F(q) versus $(\tilde{q}) = qR_c$ for various values of α

In Figure 2.5, we present a graphical representation illustrating the behavior of the static dielectric function, $F(q)$, as a function of the dimensionless wavevector $\tilde{q} = qR_c$, for different values of the parameter α. Notably, our analysis reveals a significant phenomenon: a change in sign of $F(q)$ occurs precisely at a special value of $\alpha = \alpha_c = 30$. This transition point, marked by the sign change of $F(q)$, holds pivotal significance in understanding the behavior of the system.

The change in sign of $F(q)$ at $\alpha = \alpha_c$ indicates a critical transition in the system's response to external perturbations. This critical point signifies the onset of a DWI, where the system becomes highly susceptible to density fluctuations and the emergence of spatially modulated phases. The transition from positive to negative values of $F(q)$ reflects a change in the dominant mode of the system's response, marking the transition from a stable to an unstable regime.

Moreover, the occurrence of the sign change at $\alpha = \alpha_c$ suggests the presence of enhanced correlation effects and collective behavior within the system. As α approaches α_c, correlations between particles become more pronounced, leading to a breakdown in the system's symmetry and the potential formation of ordered phases.

Overall, the behavior of $F(q)$ in Figure 2.5 provides valuable insights into the dynamic and thermodynamic properties of the system, shedding light on the onset of DWI and the emergence of spatially modulated phases. By comprehensively understanding the implications of the sign change in $F(q)$ at $\alpha = \alpha_c$, we gain deeper insights into the collective behavior and phase transitions exhibited by the system, paving the way for further exploration and applications in condensed matter physics.

Chapter 3

Bi-wire system

In this chapter, we explore a bi-wire system consisting of two parallel single-wire systems of Rydberg-dressed bosons, separated by a distance d. This setup allows us to investigate the inter-wire interactions.

When examining bosons featuring repulsive soft-core Rydberg-dressed interactions confined in two wires, the intra-wire and inter-wire interactions in real space are described[42].

This system is characterized by the following first-quantized Hamiltonian:

$$H = -\frac{\hbar^2}{2m} \sum_{l,i} \nabla^2_{r_i^l} + \sum_{l} \sum_{i<j} V_s \left| r_i^l - r_j^l \right| + \sum_{i,j} V_d \left| r_i^1 - r_j^2 \right| \tag{3.1}$$

In this context, m represents the mass of the particle, $l = 1, 2$ denotes the index for the wires, r_i^l signifies the position of the ith particle in wire l, and the intra-wire $V_s(r)$ and inter-wire $V_d(r)$ interactions in real space which will be discussed in the following[24].

3.1 Soft-core bosons in bi-wire

Inter-wire interaction is given by:

$$V_d(r) = \frac{U}{1 + \left(\frac{\sqrt{r^2+d^2}}{R_c}\right)^6} \tag{3.2}$$

Here, r represents the distance between atoms within the same wire, and d is the separation distance between the two wires. The parameters U and R_c are the interaction strength and the soft-core radius, respectively, which are dependent on parameters such as Raman coupling, red detuning, and van der Waals coefficients [13, 15, 43].

The soft-core radius of interaction R_c is defined as $R_c = \left(\frac{C_6}{2\hbar\Delta}\right)^{1/6}$ and the interaction strength U is given by $U = \left(\frac{\Omega}{2\Delta}\right)^4 \left|\frac{C_6}{R_c^6}\right|$.

In these equations Ω, $\Delta < 0$, and $C_6 < 0$ are the effective Raman coupling, red detuning, and averaged van der Waals coefficient, respectively[21].

The soft-core radius of interaction, denoted as R_c, is determined by the averaged van der Waals coefficient C_6 and the red detuning Δ. Additionally, the interaction strength U depends on the same parameters along with the effective Raman coupling Ω.

The form of the inter-wire interaction $V_d(r)$ reflects the soft-core nature of the Rydberg-dressed potential, characterized by a flat core and a van der Waals tail at long distances. This interaction is essential for understanding the collective behavior of the bosons in the bi-wire system.

By manipulating parameters such as Ω, Δ, and C_6, we can tune the interaction strength and range, thereby exploring different regimes of physical behavior. This flexibility is crucial for studying various phenomena, including the emergence of collective modes, density-wave instabilities, and other exotic states in low-dimensional quantum systems.

To analyze the interactions in momentum space, we consider the Fourier transform of the potential $V_d(r)$:

$$V_d(q) = 2UR_c \int_0^{\infty} dx \frac{\cos(qR_c x)}{1 + \left(x^2 + \left(\frac{d}{R_c}\right)^2\right)^3} \tag{3.3}$$

For convenience, we introduce the dimensionless variables $qR_c = \tilde{q}$ and $\frac{d}{R_c} = \tilde{d}$. The integral for $V_d(q)$ needs to be evaluated numerically due to its complexity.

Using the inter-wire interaction $V_d(q)$ and the intra-wire interaction $V_s(q)$ from the previous chapter, we define the symmetric and anti-symmetric components of the interaction as:

$$V_{\pm}(q) = V_s(q) \pm V_d(q) \tag{3.4}$$

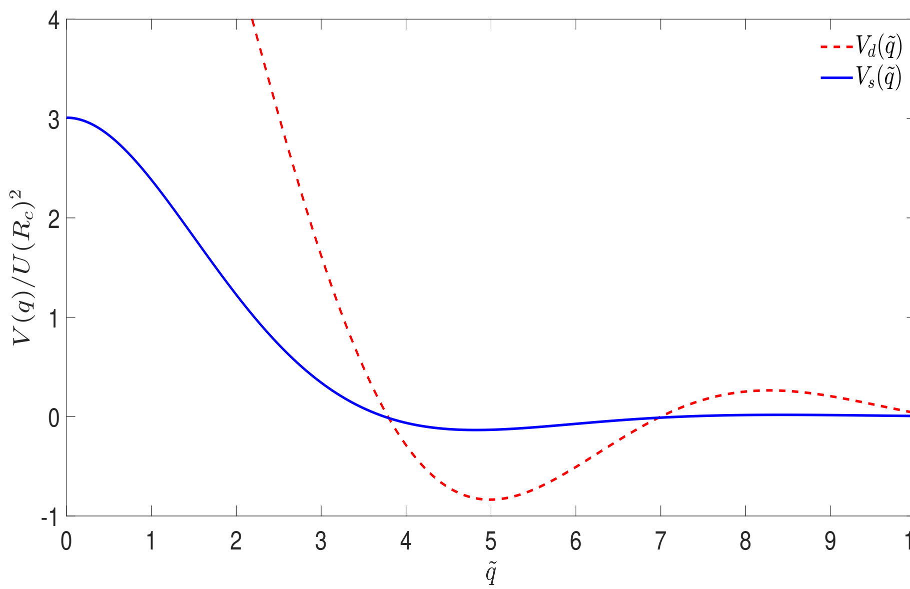

Figure 3.1: The Fourier transforms of the intra-wire and inter-wire Rydberg-dressed interactions versus $\tilde{q}$. Plot of $V_s(\tilde{q})$ and $V_d(\tilde{q})$ versus $\tilde{q}$ for $\tilde{d} = 0.1$, where $V_s(\tilde{q})$ and $V_d(\tilde{q})$ are scaled by $U(R_c)^2$

These are the symmetric and anti-symmetric components of the interaction. These components are crucial for understanding the collective excitations in the bi-wire system. The symmetric component $V_+(q)$ and the anti-symmetric component $V_-(q)$ correspond to oscillations of the density in both wires.

Figures 3.1 and 3.2 illustrates the wavevector dependence of $V_s(\tilde{q})$ and $V_d(\tilde{q})$ versus $\tilde{q}$ for various values of $\tilde{d}$. These plots provide insight into how the interaction potentials change with wavevector and inter-wire distance, highlighting the regions of stability and potential instabilities in the system.

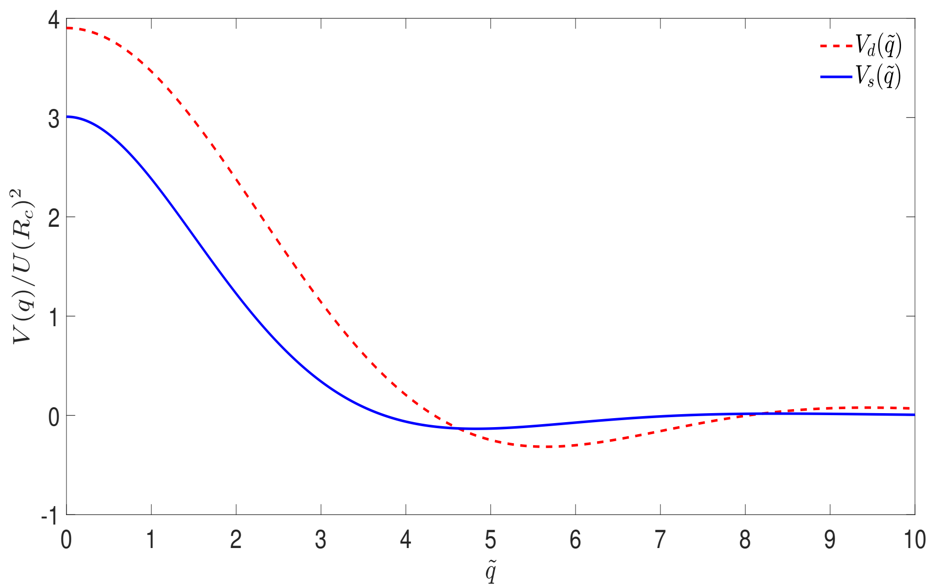

Figure 3.2: The Fourier transforms of the intra-wire and inter-wire Rydberg-dressed interactions versus $\tilde{q}$. Plot of $V_s(\tilde{q})$ and $V_d(\tilde{q})$ versus $\tilde{q}$ for $\tilde{d} = 0.5$, where $V_s(\vec{q})$ and $V_d(\tilde{q})$ are scaled by $U(R_c)^2$

3.2 Density-wave instability

When investigating the density-wave instability, a crucial component is the density-density response function, denoted as:

$$\chi_{\pm}(q,\omega) = \frac{\chi_0(q,\omega)}{1 - V_{\pm}(q)\chi_0(q,\omega)} \tag{3.5}$$

where $\chi_+(q,\omega)$ and $\chi_-(q,\omega)$ represent the response function for the symmetric and anti-symmetric modes, respectively, $V_+(q)$ and $V_-(q)$ are the symmetric and anti-symmetric components of the interaction.

And $\chi_0(q,\omega)$, is defined as:

$$\chi_0(q,\omega) = \frac{2n\epsilon_q}{\hbar^2\omega^2 - \epsilon_q^2} \tag{3.6}$$

where ϵ_q is the dispersion of free bosons, and n is the particle density in each wire (assumed to be the same for both wires).

The dispersion relation for free bosons is given by:

$$\epsilon_q = \frac{\hbar^2 q^2}{2m} \tag{3.7}$$

Then, the excitation spectrum is obtained from the solution of the following equation by employing the BdG approximation, a powerful framework widely utilized in the study of bosonic systems.

$$1 - V_{\pm}(q)\chi_0(q,\omega) = 0 \tag{3.8}$$

Solving this equation gives the excitation spectrum:

$$\hbar\omega_{\pm} = \sqrt{\epsilon_q^2 + 2n\epsilon_q V_{\pm}(q)} \tag{3.9}$$

This spectrum describes the collective excitations in the bi-wire system, with the ω_+ mode corresponding to the symmetric oscillations and the ω_- mode corresponding to the anti-symmetric oscillations. The presence of $V_{\pm}(q)$ modifies the dispersion relation, indicating the impact of inter-wire interactions on the collective behavior of the system.

The investigation of the density-density response function and the resulting excitation spectrum provides deep insights into the stability and dynamic properties of the bi-wire system. Numerical evaluations of the interaction potentials and response functions are essential for capturing the full complexity of the system and predicting experimental outcomes.

Figure 3.3 shows the dispersions of symmetric ω_+ and anti-symmetric ω_- modes of a Rydberg-dressed boson bi-wire, presented in units of $\hbar^2/(2mR_c^2)$, for different values of the inter-wire distances. Here, we consider two distinct scenarios:

1. $\alpha = 15$, which is close to the density-wave instability region at small wire spacings
2. $\alpha = 20$, where the vanishing of the roton energy is evident

The plot depicts $\frac{\hbar\omega_\pm(\tilde{q})}{E_0}$ versus $\tilde{q}$ for various values of α and $\tilde{d}$. It highlights the modes' behavior as the inter-wire distance and coupling strength vary.

Particularly noteworthy are the examples where the ω_+ and ω_- branches become zero, indicating critical points or instabilities in the system. These points of vanishing excitation energy offer valuable insights into the phase transitions and collective behavior of the bi-wire system.

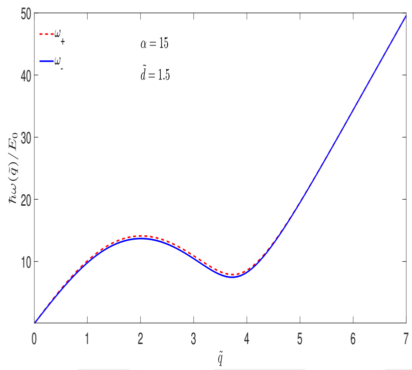

(a) $\alpha = 15$ and $\tilde{d} = 1.5$

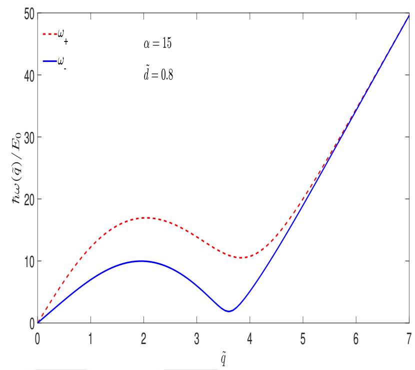

(b) $\alpha = 15$ and $\tilde{d} = 0.8$

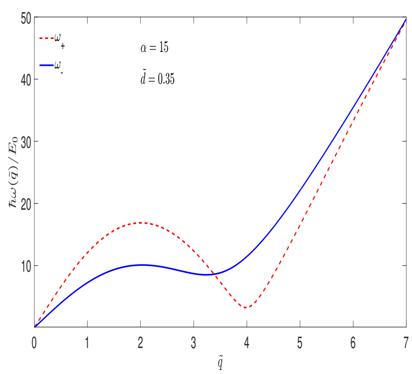

(c) $\alpha = 15$ and $\tilde{d} = 0.35$

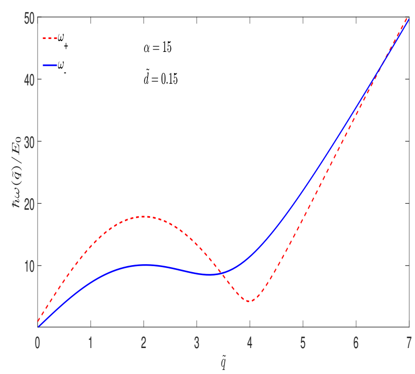

(d) $\alpha = 15$ and $\tilde{d} = 0.15$

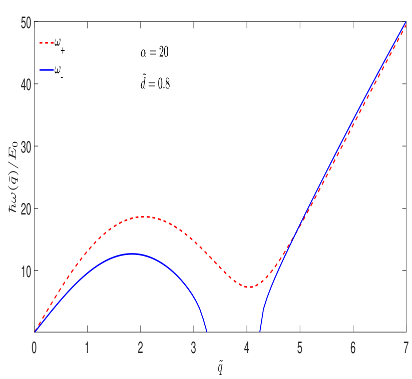

(e) $\alpha = 20$ and $\tilde{d} = 0.8$

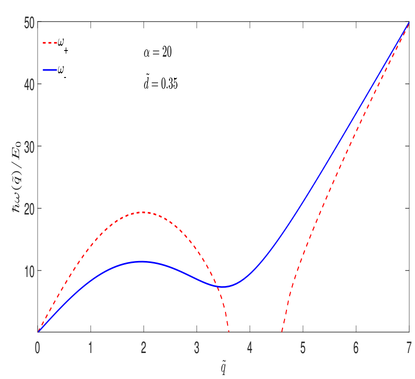

(f) $\alpha = 20$ and $\tilde{d} = 0.35$

Figure 3.3: Plots of $\frac{\hbar\omega_{\pm}(\tilde{q})}{E_0}$ versus $\tilde{q}$ for various values of α and $\tilde{d}$

3.3 Symmetric and asymmetric collective modes

The dispersion of quasiparticle excitation branches exhibits intriguing characteristics in the Rydberg-dressed boson bi-wire system. While the behavior appears linear for long wavelengths and free particles (i.e., quadratic) for large wave vectors, intermediate q values reveal distinctive maxon-roton features, especially under strong coupling conditions [15, 61]. Remarkably, these features are already discernible in the basic BdG approximation, highlighting the profound influence of Rydberg-dressed interactions on the system's collective behavior and excitations.

Figure 3.3 visually presents the dispersion of symmetric and asymmetric collective modes in a bi-wire system consisting of Rydberg-dressed bosons. Across multiple subfigures, we keep the coupling constant α constant while varying the wire separation. This allows us to highlight the influence of inter-wire coupling on mode dispersion. Notably, when the wire separation is substantial (i.e., $d \gg R_c$), the two wires behave almost independently, leading to the degeneracy of the two collective mode branches. This observation underscores the critical role of inter-wire coupling in shaping the collective behavior of the bi-wire system.

For the selected values of α in this context, the roton minima are already discernible within the density mode ω_+ of two independently decoupled wires. As we reduce the separation between the wires, the asymmetric mode ω_- becomes increasingly softened. At smaller distances, the contribution of the asymmetric component of the interaction $V_-(q)$ diminishes, and the asymmetry mode's dispersion adopts a free-particle-like behavior (as observed, for instance, in the subfigure (d)). In this regime, the roton in the total density mode becomes remarkably soft, nearly resembling the density mode of a single-wire with a coupling constant of 2α. The energy associated with both roton minima exhibits non-monotonic variations with changes in wire spacing. The disappearance of the roton minima for $\alpha = 20$ in subfigure (e), observed at $\tilde{d} = 0.8$ and $\tilde{d} = 0.35$ in subfigure (f), signifies a density-wave instability in the asymmetry and symmetric channels, respectively.

Another noteworthy observation is that two modes converge at finite wave vectors where $V_d(q) = 0$. This convergence loses its degeneracy when the symmetry between the two wires is disrupted, for instance, through density imbalance or a finite counterflow. This phenomenon highlights the sensitivity of the mode behavior to the system's symmetry and dynamic conditions, underscoring the intricate interplay between inter-wire coupling and external perturbations.

As depicted in Figure 3.3 subfigures (e) and (f), at high coupling strengths, the energy associated with the roton tends towards zero, and eventually, the energy of quasiparticle excitations may become imaginary. This signifies the instability of the homogeneous superfluid phase towards density-waves within specific ranges of wire spacing. Such behavior underscores the intricate balance between inter-wire coupling and collective excitations, leading to the emergence of density-wave instabilities under certain conditions.

3.4 Density-density response function

The static density response function $\chi_{\pm}(q)$ is a crucial quantity in understanding a system's collective excitations and screening properties. It is given by:

$$\chi_{\pm}(q) = \frac{\chi_0(q)}{1 - V_{\pm}(q)\chi_0(q)} \tag{3.10}$$

where $\chi_0(q)$ is the density response function, and $V_{\pm}(q)$ represents the interaction potentials for the symmetric (+) and asymmetric (−) modes.

The density response function $\chi_0(q)$ is expressed as:

$$\chi_0(q) = -\frac{2n}{\epsilon_q} \tag{3.11}$$

The interaction-modified density response functions $\chi_{\pm}(q)$ reflect how the system responds to external perturbations in the presence of interactions. Figures

3.4 and 3.5 plot the scaled response functions $-\chi_-(q)UR_c$ and $-\chi_+(q)UR_c$ versus the dimensionless wave vector $\tilde{q} = qR_c$ for various values of the parameter α.

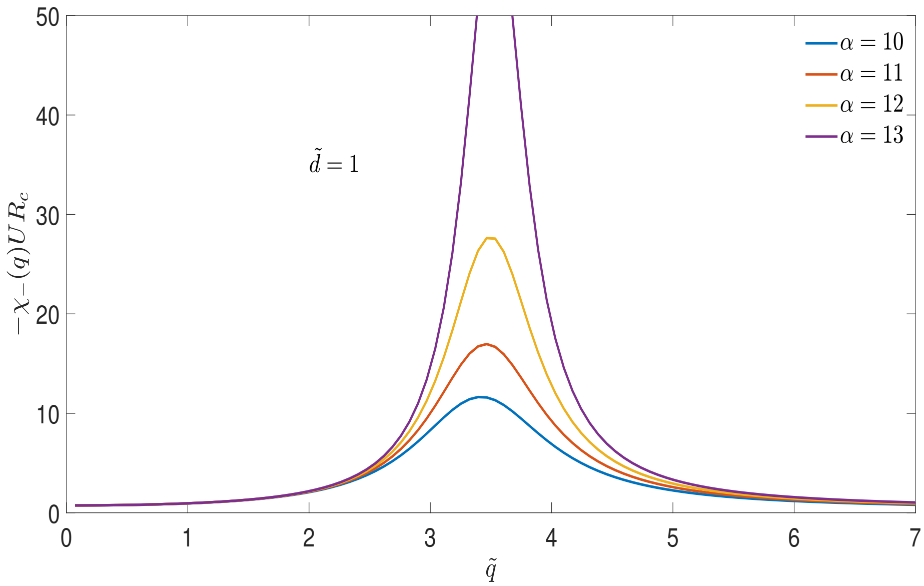

Figure 3.4: The asymmetric component of the density-density response function $-\chi_-(q)UR_c$ (in the units of $1/(UR^2c)$) within the random phase approximation versus $(\tilde{q}) = qR_c$ for various values of α

These plots demonstrate the divergence of $-\chi_\pm(q)$ at a critical value of the parameter α. This divergence indicates a phase transition or instability in the system. It is the point that roton is vanishing. The critical behavior observed in $\chi_\pm(q)$ is significant for understanding phenomena such as charge density waves or other forms of order in the system.

The divergence of the response functions at $\alpha = 13$ suggests that the system undergoes a dramatic change in its electronic properties, possibly signaling the onset of a new phase. By analyzing the behavior of $\chi_\pm(q)$ near the critical point, we can gain insights into the nature of the interactions and the resulting collective excitations.

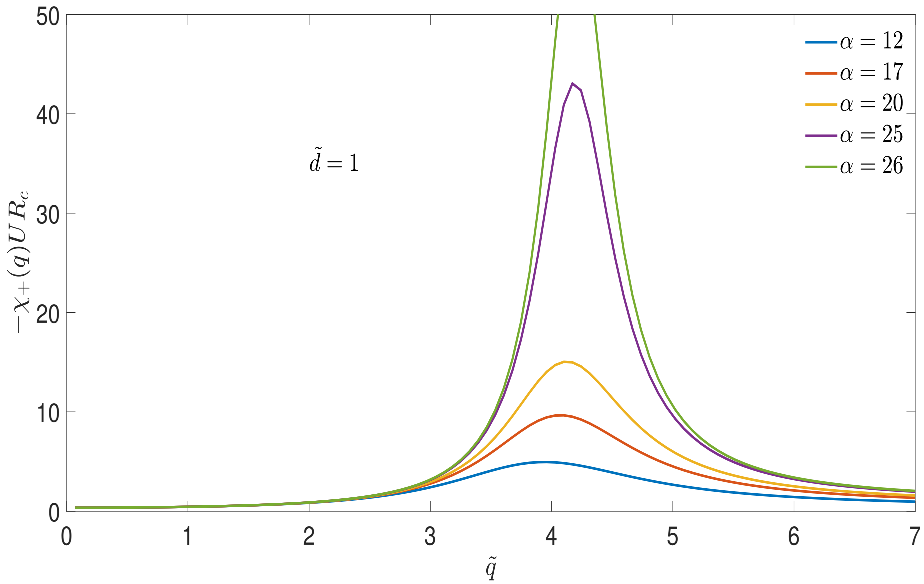

Figure 3.5: The symmetric component of the density-density response function $-\chi_+(q)UR_c$ (in the units of $1/(UR^2c)$) within the random phase approximation versus $(\tilde{q}) = qR_c$ for various values of α

3.5 Phase diagram of the bi-wire of bosons with Rydberg-dressed interaction

One intriguing avenue of research involves BECs confined to bi-wire geometries, where the interplay between wire spacing and interaction strength gives rise to diverse phase transitions and instabilities. In this section, we delve into our investigation of DW instabilities in a boson bi-wire system with interactions dressed by Rydberg states.

Our initial observations reveal intriguing behavior in the response functions of the system. We note that the symmetric component of the response function exhibits divergence at larger wire spacings, suggesting a propensity for DW instability in the density channel. Conversely, the asymmetric component displays similar behavior at smaller wire spacings, hinting at the possibility of DW instability in the asymmetric channel. This observation implies a dual susceptibility of the system to DW instabilities, with distinct manifestations in different channels depending on the wire spacing.

A key indicator of DW instability is the presence of singularities in the density-density response function. These singularities serve as hallmark signatures, signaling the potential for phase transitions leading to the formation of density-waves within the system. By analyzing the density-density response function, we can identify regions of enhanced susceptibility to DW instability, providing valuable insights into the underlying physics governing the system's behavior.

To explore these phenomena in detail, we conducted a comprehensive investigation utilizing a boson bi-wire system with interactions influenced by Rydberg states. Leveraging the tunability and control afforded by Rydberg-dressed interactions, we were able to systematically probe the emergence of DW instabilities in both the symmetric and asymmetric channels.

The observation of diverging behavior in the symmetric component of the response function at larger wire spacings and the asymmetric component at smaller wire spacings indicates distinct tendencies within the boson bi-wire system. At larger wire spacings, the symmetric response component's divergence implies a predisposition towards the emergence of DW instability in this channel. Conversely, at smaller wire spacings, the diverging behavior in the asymmetric response component suggests a propensity for DW instability in the asymmetric channel.

The occurrence of singularities in the density-density response function further corroborates the presence of density-wave instability within the system. These singularities serve as characteristic signatures, indicating the potential for the system to undergo phase transitions leading to density-wave formation.

In our investigation, we specifically focused on a boson bi-wire system where interactions are influenced by Rydberg states. This choice allowed us to explore the behavior of the system with enhanced control and tunability, providing insights into the interplay between interactions and wire structure.

The phase diagram presented in Figure 3.6 encapsulates the diverse range of phases and instabilities observed within the system. It delineates regions characterized by homogeneous superfluidity (SF), where the system exhibits uniform flow without any spatial modulation. Additionally, the phase diagram identifies regions where DW instabilities may arise, either in the symmetric channel, the asymmetric channel, or concurrently in both channels. This comprehensive depiction of the phase diagram facilitates a thorough understanding of the system's behavior under varying conditions, offering valuable insights into the complex dynamics of boson bi-wire systems with Rydberg-dressed interactions.

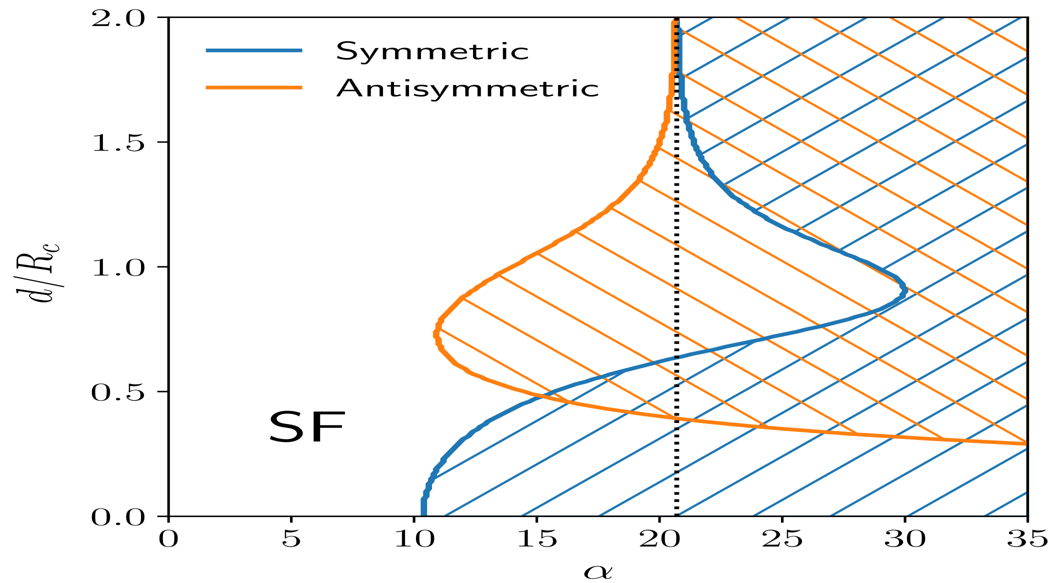

Figure 3.6: The phase diagram of a bi-wire of boson with Rydberg-dressed interaction in the $d-\alpha$ plane. The homogeneous superfluid (SF), and density-wave (DW) instability in the symmetric and asymmetric channels are marked. The vertical line at $\alpha_c \approx 21$ is the critical coupling strength for the density-wave instability of an isolated two-dimensional wire of Rydberg-dressed bosons.

Our investigation sheds light on the intricate dynamics of boson bi-wire systems with Rydberg-dressed interactions. By elucidating the susceptibility to DW instabilities in both the symmetric and asymmetric channels, we contribute to a deeper understanding of phase transitions and emergent phenomena in ultracold atomic systems.

3.6 Long wavelength excitations and sound velocity

In the study of excitations within coupled wire systems, similar principles apply as those observed in single-wire cases. The excitation spectrum can be described by the relation:

$$\hbar\omega(q) = \sqrt{\epsilon_q^2 + 2n\epsilon_q V_\pm(q)} \tag{3.12}$$

where ϵ_q represents the dispersion relation of free bosons, n denotes the particle density, and $V_\pm(q)$ represents the interaction potentials for symmetric $(+)$ and asymmetric $(-)$ modes.

In the long wavelength limit $(q \to 0)$, the dispersion relations for both symmetric and asymmetric modes exhibit linear behavior, expressed as:

$$\omega_\pm(q \to 0) \approx \nu_\pm q \tag{3.13}$$

where ν_+ and ν_- denote the sound velocities for the symmetric and asymmetric modes, respectively.

The sound velocities $\nu_\pm$ can be derived from the interaction potentials in the long wavelength limit, given by:

$$\nu_\pm = \sqrt{\frac{nV_\pm(q \to 0)}{m}} \tag{3.14}$$

with m being the mass of the particles in the system. The interaction potentials at $q = 0$ are defined as:

$$V_s(q = 0) = \frac{2UR_c\pi}{3} \tag{3.15}$$

$$V_d(q=0) = 2UR_c \int_0^\infty \frac{dx}{(1+(x^2+\tilde{d}^2)^3)} \tag{3.16}$$

where U is the interaction strength, R_c is the soft-core radius, and $\tilde{d}$ is the dimensionless separation between wires.

Figure 3.7 illustrates the dependence of the sound velocities $\nu_\pm$ on the wire separation $\tilde{d}$. The distinct behavior of the symmetric and asymmetric modes is clearly observed as $\tilde{d} \to 0$. In the limit of large wire separation ($\tilde{d} \to \infty$), the two modes converge and become degenerate, resulting in the sound velocities approaching a common value.

This analysis highlights the intricate relationship between inter-wire interactions and the propagation characteristics of excitations in coupled wire systems, providing essential insights into the fundamental behavior of such systems in various regimes of wire separation.

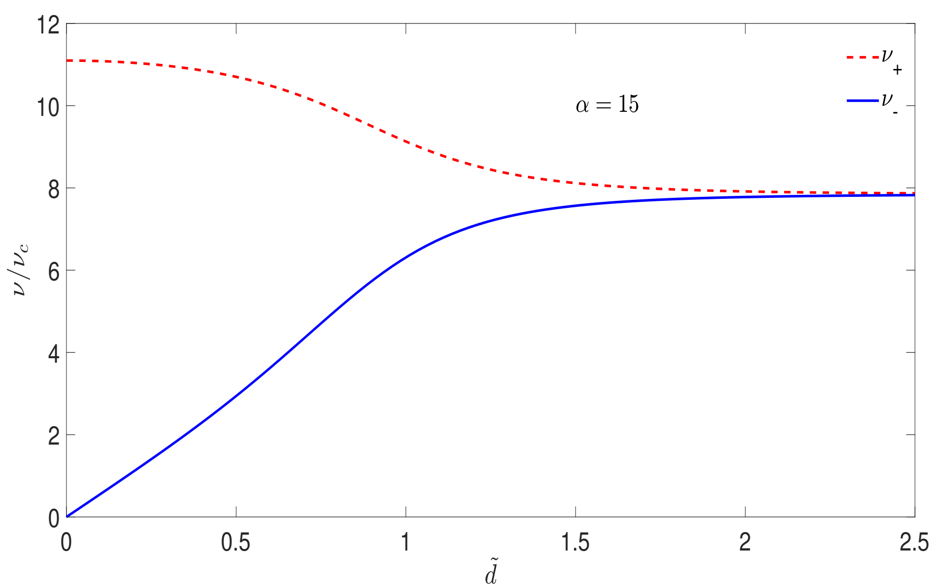

Figure 3.7: The sound velocities of symmetric and asymmetric modes (in the units of $v_c = \sqrt{\frac{\hbar}{mR_c}}$) versus $\tilde{d}$ for $\alpha = 15$.

3.7 Density imbalanced bi-wire

In this section, we consider a bi-wire system of Rydberg-dressed bosons with a density imbalance between the two wires. In this scenario, the particle density differs between the two wires, leading to unique collective excitation modes.

The collective modes of the density-imbalanced bi-wire can be determined by analyzing the following expression:

$$\hbar^2\omega_{\pm}^2(q) = \epsilon_q^2 + 2n\epsilon_q V_{\pm}(q) \pm 2n\epsilon_q\sqrt{V_d(q)^2 + P^2 V_+(q)V_-(q)} \tag{3.17}$$

where n is the average particle density, $V_{\pm}(q)$ are the interaction potentials for the symmetric $(+)$ and asymmetric $(-)$ modes, and P is the density polarization, defined as:

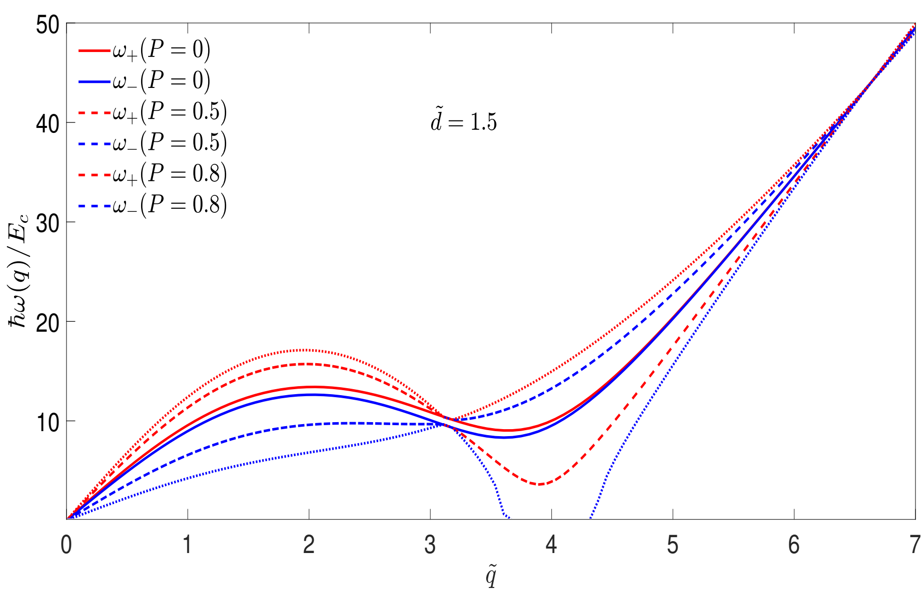

Figure 3.8: Dispersion of one mode of a density-imbalanced Rydberg-dressed boson bi-wire $\hbar\omega_{\pm}(q)$ versus $\tilde{q}$ at $\alpha = 20$ with different polarizations P and wire separation $\tilde{d} = 1.5$.

$$n = \frac{n_1 + n_2}{2} \tag{3.18}$$

$$P = \frac{n_1 - n_2}{n_1 + n_2} \tag{3.19}$$

with n_1 and n_2 being the densities in the first and second wires, respectively.

For $P = 0$, indicating no density imbalance, Equation (3.16) simplifies to Equation (3.8), which describes the symmetric and asymmetric modes in a density-balanced bi-wire.

Figures 3.8 and 3.9 present the dispersion relations of the collective modes in a density-imbalanced bi-wire. The figures illustrate $\hbar\omega_\pm(q)$ as functions of the dimensionless wave vector $\tilde{q} = qR_c$ for various values of the density polarization P [62].

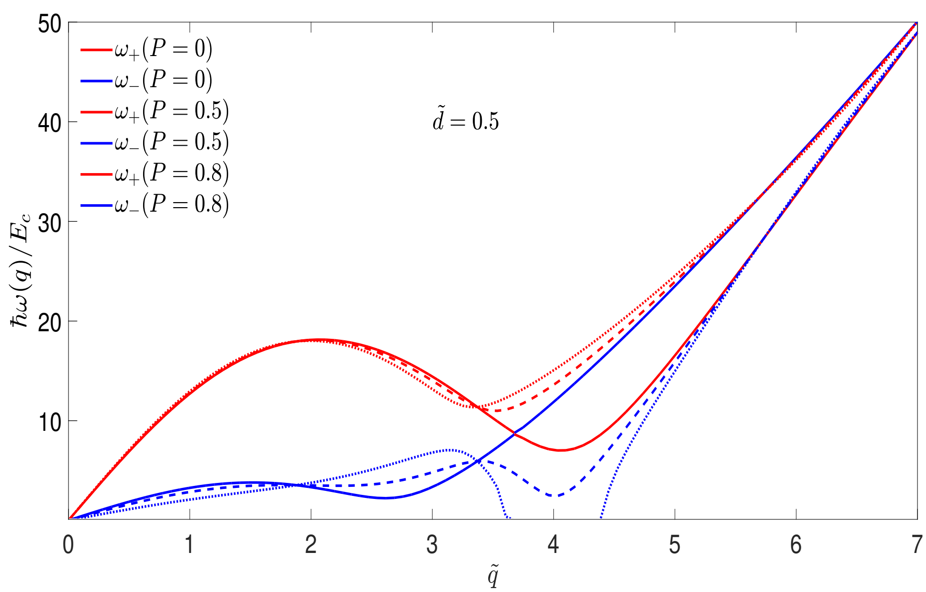

Figure 3.9: Dispersion of one mode of a density-imbalanced Rydberg-dressed boson bi-wire $\hbar\omega_\pm(q)$ versus $\tilde{q}$ at $\alpha = 20$ with different polarizations P and wire separation $\tilde{d} = 0.5$.

3.7.1 Analysis of results

The dispersion relations $\hbar\omega_\pm(q)$ reveal how the collective excitation modes are affected by the density imbalance. As the density polarization P increases, the symmetric and asymmetric modes exhibit significant changes:

- Symmetric mode (ω_+): This mode is generally associated with in-phase oscillations of particles in both wires. The presence of a density imbalance modifies its dispersion, particularly at low wave vectors.
- Asymmetric mode (ω_-): This mode involves out-of-phase oscillations between the wires. The density imbalance causes more pronounced modifications in its dispersion, potentially leading to new instability regimes or altered propagation characteristics.

The critical insights gained from these dispersion relations can help understand density-imbalanced bi-wires' stability and dynamic properties. These properties are crucial for potential applications in quantum information processing and condensed matter physics, where control over collective excitations is essential.

Chapter 4

Conclusion

We have examined the dispersions of collective modes within single-wire and double-wire structures of bosons interacting via Rydberg-dressed interactions. In the long-wavelength regime, both symmetry and asymmetry modes exhibit linear behavior in wave vectors, each with distinct sound velocities. At intermediate wave vector values, a maxon-roton feature becomes apparent in both branches, particularly prominent at large coupling constants. Additionally, we investigated the influence of wire spacing on mode dispersion. Smaller wire spacings result in the disappearance of the asymmetric mode, characterized by a dispersion akin to free particles. As wire spacing increases, the coupling between the wires diminishes, leading to the degeneracy of two modes in symmetric bi-wires. At strong couplings, the homogeneous system becomes prone to instability towards density waves, indicated by the disappearance of the roton energy. This instability can manifest in either or both symmetry and asymmetry branches.

The density imbalance between the two wires increases and decreases the energy of the upper and lower excitation branches, respectively. The density imbalance makes the homogeneous SF phase unstable at smaller coupling constants.

We should note that although the roton softening, we find from BdG approximation signals the instability of homogeneous system to density-modulated phases, the true nature of the inhomogeneous phases are revealed through more sophisticated numerical techniques such as the Gross-Pitaevskii or Quantum Monte Carlo methods. Such calculations are beyond the scope of our current work. Still, previous numerical studies of Rydberg-dressed Bose gases at both two and three dimensions suggest that BdG approximation is indeed very good in giving the proper qualitative picture of the phase transitions. [15, 18, 25, 26]

In conclusion, our investigation focused on the dispersions of collective modes within single-wire and double-wire structures of bosons with Rydberg-dressed interactions. In the long-wavelength limit, both symmetry and asymmetry modes exhibit linear behavior in wave vectors with differing sound velocities. Notably, a maxon-roton feature emerges in both branches at high coupling constants. We also explored the impact of wire spacing on mode dispersion, finding that at smaller spacings, the asymmetric mode vanishes, characterized by free-particle-like dispersion. Increasing spacing nearly decouples the wires, leading to mode degeneracy in symmetric bi-wires. Moreover, at strong couplings, the homogeneous system becomes prone to instability toward density waves, indicated by roton energy vanishing. This instability can manifest in either or both symmetry and asymmetry branches.

Furthermore, a finite superfluid counterflow induces energy changes in the upper and lower excitation branches, respectively, akin to the effect of density imbalance between wires. Both counterflow and density imbalance render the homogeneous superfluid phase unstable at lower coupling constants. Recent experimental advancements promise that some concepts explored in this study could be validated in laboratory settings. [1, 2]

Moving forward, it would be valuable to extend our analysis to include the effects of external perturbations or additional degrees of freedom, such as spin-orbit coupling or magnetic fields, which can significantly impact the collective behavior of the system. Furthermore, exploring the dynamic response of Rydberg-dressed bosons to time-dependent perturbations or driving fields could shed light on novel phenomena such as dynamical phase transitions or the emergence of exotic steady states. Additionally, incorporating finite temperature effects and beyond-mean-field corrections in future studies would provide a more comprehensive understanding of the thermal and quantum fluctuations in Rydberg-dressed systems.

Moreover, the insights gained from our theoretical investigation could inspire new experimental setups aimed at probing the collective behavior of Rydberg-dressed bosons with unprecedented precision. Advancements in experimental techniques, such as quantum gas microscopy and cavity quantum electrodynamics, offer exciting opportunities for directly observing and manipulating individual Rydberg atoms in optical lattices or trap arrays. These experimental platforms could provide crucial validation for our theoretical predictions and pave the way for engineering novel quantum states with tailored interactions and geometries.

Overall, the exploration of Rydberg-dressed bosonic systems represents a fascinating frontier in quantum physics, offering rich opportunities for both fundamental research and practical applications in quantum technologies. By continuing to bridge theory and experiment, we can unlock the full potential of these exotic quantum fluids and harness their unique properties for future advancements in quantum science and technology.

Bibliography

[1] G. Browaeys and T. Lahaye, "Many-Body Physics with Individually-Controlled Rydberg Atoms," *Nature Physics*, vol. 16, no. 132, 2020.

[2] S. de eeseleuc, V. Lienhard, P. Scholl, D. Barredo, S. Weber, N. Lang, H. P. Buchler, T. Lahaye, and A. Browaeys, "Experimental realization of a symmetry protected topological phase of interacting bosons with rydberg atoms," *Science*, vol. 365, no. 775, 2019.

[3] A. Browaeys, D. Barredo, and T. Lahaye, "Experimental investigations of dipole-dipole interactions between a few rydberg atoms," *Journal of Physics B: Atomic, Molecular and Optical Physics*, vol. 49, no. 152001, 2016.

[4] H. Labuhn, D. Barredo, S. Ravets, S. D. Leseleuc, T. Macri, T. Lahaye, and A. Browaeys, "Tunable two-dimensional arrays of single rydberg atoms for realizing quantum ising models," *Nature*, vol. 534, no. 667, 2016.

[5] H. Weimer, M. Muller, I. Lesanovsky, P. Zoller, and H. P. Buchler, "A rydberg quantum simulator," *Nature Physics*, vol. 6, no. 382, 2010.

[6] P. Scholl, M. Schuler, H. J. Williams, A. A. Eberharter, D. Barredo, K.-N. Schymik, V. Lienhard, L.-P. Henry, T. C. Lang, T. Lahaye, *et al.*, "Programmable quantum simulation of 2d antiferromagnets with hundreds of rydberg atoms," *Nature*, vol. 595, no. 233, 2021.

[7] M. Saffman, T. G. Walker, and K. Molmer, "Quantum information with rydberg atoms," *Reviews of Modern Physics*, vol. 82, no. 2313, 2010.

[8] Y. Y. Jau, A. Hankin, T. Keating, I. Deutsch, and G. Biedermann, "Entangling atomic spins with a strong rydberg-dressed interaction," *Nature Physics*, vol. 12, no. 71, 2016.

[9] M. Morgado and S. Whitlock, "Quantum simulation and computing with rydberg-interacting qubits," *AVS Quantum Science*, vol. 3, no. 023501, 2021.

[10] T. Peyronel, O. Firstenberg, Q. Y. Liang, S. Hoerberth, A. V. Gorshkov, T. Pohl, M. D. Lukin, and V. Vuletic, "Quantum nonlinear optics using cold atomic ensembles," *Nature*, vol. 488, no. 57, 2012.

[11] O. Firstenberg, C. S. Adams, and S. Hoerberth, "Nonlinear quantum optics mediated by rydberg interactions," *Journal of Physics B: Atomic, Molecular and Optical Physics*, vol. 49, no. 152003, 2016.

[12] N. L. R. Spong, Y. Jiao, O. D. W. Hughes, K. J. Weatherill, I. Lesanovsky, and C. S. Adams, "A collectively encoded rydberg qubit," *Physical Review Letters*, vol. 127, no. 063604, 2021.

[13] J. E. Johnson and S. L. Rolston, "Interactions between rydberg-dressed atoms," *Physical Review A*, vol. 82, no. 033412, 2010.

[14] J. B. Balewski, A. T. Krupp, A. Gaj, S. Hoerberth, R. Low, and T. Pfau, "Rydberg dressing: Understanding of collective many-body effects and implications for experiments," *New Journal of Physics*, vol. 16, no. 063012, 2014.

[15] N. Henkel, R. Nath, and T. Pohl, "Three-dimensional roton excitations and supersolid formation in rydberg-excited bose-einstein condensates," *Physical Review Letters*, vol. 104, no. 195302, 2010.

[16] A. W. Glaetzle, R. Nath, B. Zhao, G. Pupillo, and P. Zoller, "Driven-dissipative dynamics of a strongly interacting rydberg gas," *Physical Review A*, vol. 86, no. 043403, 2012.

[17] M. Mayle, I. Lesanovsky, and P. Schmelcher, "Dressing of ultracold atoms by their rydberg states in an ioffe–pritchard trap," *Journal of Physics B: Atomic, Molecular and Optical Physics*, vol. 43, no. 155003, 2010.

[18] F. Cinti, T. Macri, W. Lechner, G. Pupillo, and T. Pohl, "Defect-induced supersolidity with soft-core bosons," *Nature Communications*, vol. 5, no. 1, 2014.

[19] N. Henkel, F. Cinti, P. Jain, G. Pupillo, and T. Pohl, "Supersolid vortex crystals in rydberg-dressed bose-einstein condensates," *Physical Review Letters*, vol. 108, no. 265301, 2012.

[20] W. H. Li, T. C. Hsieh, C. Y. Mou, and D. W. Wang, "Emergence of a metallic quantum solid phase in a rydberg-dressed fermi gas," *Physical Review Letters*, vol. 117, no. 035301, 2016.

[21] I. Seydi, S. H. Abedinpour, R. Asgari, M. Panholzer, and B. Tanatar, "Rydberg-dressed fermi liquid: Correlations and signatures of droplet crystallization," *Physical Review A*, vol. 103, no. 043308, 2021.

[22] M. Teruzzi, C. Apostoli, D. Pini, D. E. Galli, and G. Bertaina, "Evolution of static and dynamical density correlations in a one-dimensional soft-core gas from the tonks-girardeau limit to a clustering fluid.," *arXiv preprint*, no. 2106.11832, 2021.

[23] R. Verresen, M. D. Lukin, and A. Vishwanath, "Prediction of toric code topological order from rydberg blockade," *Physical Review X*, vol. 11, no. 031005, 2021.

[24] A. Keles, E. Zhao, and X. Li, "f-wave superfluidity from repulsive interaction in rydberg-dressed fermi gas," *Physical Review A*, vol. 101, no. 023624, 2020.

[25] I. Seydi, S. H. Abedinpour, R. E. Zillich, R. Asgari, and B. Tanatar, "Rotons and bose condensation in rydberg-dressed bose gases," *Physical Review A*, vol. 101, no. 013628, 2020.

[26] T. Macri, S. Saccani, and F. Cinti, "Ground state and excitation properties of soft-core bosons," *Journal of Low Temperature Physics*, vol. 177, no. 59, 2014.

[27] M. Burrello, I. Lesanovsky, and A. Trombettoni, "Reaching the quantum hall regime with rotating rydberg-dressed atoms," *Physical Review Research*, vol. 2, no. 023290, 2020.

[28] C. H. Hsueh, C. W. Wang, and W. C. Wu, "Vortex structures in a rotating rydberg-dressed bose-einstein condensate with the lee-huang-yang correction," *Physical Review A*, vol. 102, no. 063307, 2020.

[29] D. Petter, G. Natale, R. M. W. van Bijnen, A. Patscheider, M. J. Mark, L. Chomaz, and F. Ferlaino, "Probing the roton excitation spectrum of a stable dipolar bose gas," *Physical Review Letters*, vol. 122, no. 183401, 2019.

[30] L. Chomaz, R. M. van Bijnen, D. Petter, G. Faraoni, S. Baier, J. H. Becher, M. J. Mark, F. Waechtler, L. Santos, and F. Ferlaino, "Observation of roton mode population in a dipolar quantum gas," *Nature Physics*, vol. 14, no. 442, 2018.

[31] A. Boudjemaa and G. V. Shlyapnikov, "Two-dimensional dipolar bose gas with the roton-maxon excitation spectrum," *Physical Review A*, vol. 87, no. 025601, 2013.

[32] Y. Chen, M. Kadic, and M. Wegener, "Roton-like acoustical dispersion relations in 3d metamaterials," *Nature Communications*, vol. 12, no. 1, 2021.

[33] L. Santos, G. V. Shlyapnikov, and M. Lewenstein, "Roton-maxon spectrum and stability of trapped dipolar bose-einstein condensates," *Physical Review Letters*, vol. 90, no. 250403, 2003.

[34] H. Lyu and Y. Zhang, "Spin-orbit-coupling-assisted roton softening and superstripes in a rydberg-dressed bose-einstein condensate," *Physical Review A*, vol. 102, no. 023327, 2020.

[35] C. Hsueh, Y. Tsai, K. Wu, M. Chang, and W. C. Wu, "Pseudospin orders in the supersolid phases in binary rydberg-dressed bose-einstein condensates," *Physical Review A*, vol. 88, no. 043646, 2013.

[36] E. Akaturk, S. H. Abedinpour, and B. Tanatar, "Density-wave instability and collective modes in a bilayer system of antiparallel dipoles," *Journal of Physics Communications*, vol. 2, no. 015018, 2018.

[37] A. Macia, G. E. Astrakharchik, F. Mazzanti, S. Giorgini, and J. Boronat, "Single-particle versus pair superfluidity in a bilayer system of dipolar bosons," *Physical Review A*, vol. 90, no. 043623, 2014.

[38] M. Hebenstreit, M. Rader, and R. E. Zillich, "Dipolar bilayer with antiparallel polarization with a self-bound liquid," *Physical Review A*, vol. 93, no. 013611, 2016.

[39] F. Cinti, D. W. Wang, and M. Boninsegni, "Phases of dipolar bosons in a bilayer geometry," *Physical Review A*, vol. 95, no. 023622, 2017.

[40] M. Callegari, M. M. Parish, and F. M. Marchetti, "Dipolar fermions in a multilayer geometry," *Physical Review B*, vol. 95, no. 085124, 2017.

[41] R. K. Moudgil, P. K. Ahluwalia, and K. N. Pathak, "Ground state of a double-layer charged bose system," *Physical Review B*, vol. 56, no. 14776, 1997.

[42] R. Khasseh, S. H. Abedinpour, and B. Tanatar, "Phase diagram and dynamics of rydberg-dressed fermions in two dimensions," *Physical Review A*, vol. 96, no. 053611, 2017.

[43] J. Honer, H. Weimer, T. Pfau, and H. P. Buchler, "Collective many-body interaction in rydberg dressed atoms," *Physical Review Letters*, vol. 105, no. 160404, 2010.

[44] P. G. de Gennes, *Superconductivity of Metals and Alloys.* Perseus, 1999.

[45] G. Mayan and Z. Haghshenasfard, *Many-Body Theory of Condensed Matter Systems: An Introductory Course.* Cambridge University Press, 2020.

[46] S. M. Girvin and K. Yang, *Modern Condensed Matter Physics.* Cambridge University Press, 2019.

[47] A. R. P. Lima and A. Pelster, "Beyond mean-field low-lying excitations of dipolar bose gases," *Physical Review A*, vol. 86, no. 063609, 2012.

[48] L. Pitaevskii and S. Stringari, *Bose-Einstein condensation and superfluidity*, vol. 164. Oxford University Press, 2016.

[49] S. H. Abedinpour and B. Tanatar, "Counterflow in bose gas bilayers: Collective modes and dissipationless drag," *Low Temperature Physics*, vol. 46, no. 480484, 2020.

[50] B. Tanatar and A. K. Das, "Drag effect for a bilayer charged-bose-gas system," *Phys. Rev. B*, vol. 54, no. 1382731, 1996.

[51] V. Borish, O. Markovic, J. A. Hines, S. V. Rajagopal, and M. Schleier-Smith, "Transverse-field Ising dynamics in a Rydberg-dressed atomic gas," *Phys. Rev. Lett.*, vol. 124, no. 063601, 2020.

[52] J. M. Munoz, R. Sawant, A. Maffei, X. Wang, and G. Barontini, "Realizing the Frenkel-Kontorova model with Rydberg-dressed atoms," *Phys. Rev. A*, vol. 102, no. 043308, 2020.

[53] T. Sheng, J. Qian, X. Li, Y. Niu, and S. Gong, "Quantum simulation of the Unruh effect with a Rydberg-dressed Bose-Einstein condensate," *Phys. Rev. A*, vol. 103, no. 013301, 2021.

[54] S. Sevincli, N. Henkel, C. Ates, and T. Pohl, "Nonlocal nonlinear optics in cold Rydberg gases," *Phys. Rev. Lett.*, vol. 107, no. 153001, 2011.

[55] M. Plodzien, G. Lochead, J. de Hond, N. J. van Druten, and S. Kokkelmans, "Rydberg dressing of a one-dimensional Bose-Einstein condensate," *Phys. Rev. A*, vol. 95, no. 043606, 2017.

[56] J. M. Duan and S. Yip, "Supercurrent drag via the coulomb interaction," *Phys. Rev. Lett.*, vol. 70, no. 364750, 1993.

[57] J. M. Duan, "Nature of coupling mechanisms between pancake vortices in neighboring superconducting layersn," *Phys. Rev. B*, vol. 49, no. 625264, 1994.

[58] G. Baym and C. J. Pethick, "Landau critical velocity in weakly interacting bose gases," *Phys. Rev. A*, vol. 86, no. 023602, 2012.

[59] K. Singer, J. Stanojevic, M. Weidemüller, and R. Cote, "Long-range interactions between alkali Rydberg atom pairs correlated to the ns–ns, np–np and nd–nd asymptotes," *J.Phys. B: At. Mol. Opt. Phys.*, vol. 38, no. S295, 2005.

[60] A. Arias, G. Lochead, T. M. Wintermantel, S. Helmrich, and S. Whitlock, "Realization of a Rydberg-dressed ramsey interferometer and electrometer," *Phys. Rev. Lett.*, vol. 122, no. 053601, 2019.

[61] G. McCormack, R. Nath, and W. Li, "Dynamical excitation of maxon and roton modes in a rydberg-dressed bose-einstein condensate," *Physical Review A*, vol. 102, no. 023319, 2020.

[62] F. Pouresmaeeli, S. H. Abedinpour, and B. Tanatar, "Density and pseudo-spin rotons in a bilayer of soft-core bosons," *Journal of Physics B*, vol. 56, no. 125001, 2023.